PAPER

Check for updates

Antifungal and antibacterial investigation of quinary Zr Al Fe Co Ni layered double hydroxide and its Al Fe Co Ni quaternary and Fe Co Ni tertiary roots

Rehab Mahmoud,*[a] Zienab E. Eldin,[b] Ashraf Khalifa,[cd] Alaa A. Ahmed Anwar,[a] Yasser GadelHak, [b] Sarah I. Othman,[e] Ahmed A. Allam,[f] Doaa Essam,[a] Fatma I. Abo El-Ela,[g] Sahar Abdel Aleem Abdel Aziz[h] and Amal Zaher[i]

Layered double hydroxides (LDH) are promising 2D nanomaterials being investigated for several engineering and biomedical applications. In this work, quinary Zr Al Fe Co Ni LDH and its Al Fe Co Ni LDH quaternary and Fe Co Ni LDH tertiary roots were prepared and characterized. All samples showed an aggregated, layered morphology with zero surface charge and approximately 300 nm of hydrodynamic size. BET surface area of Al Fe Co Ni LDH showed a remarkable value of 143.25 m^2 g^{-1} as opposed to 26.2 m^2 g^{-1} and 45.4 m^2 g^{-1} for Fe Co Ni LDH and Zr Al Fe Co Ni LDH, respectively. The antimicrobial activity of the prepared samples was assessed against the many pathogenic bacteria; *Bacillus* (*B.*) *subtilis*, *Escherichia* (*E.*) *coli*, *Haemophilus* (*H.*) *influenza*, *Listeria* (*L.*) *monocytogenes*, *Staphylococcus* (*S.*) *aureus*, and *Streptococcus* (*St.*) *pneumonia*, and six fungal species. Furthermore, anti-biofilm activity, growth curve assay, and effect of UV illumination were examined against various pathogenic microbes. Zr Al Fe Co Ni displayed remarkable antibacterial activity, as indicated by the lowest values of the minimum inhibitory concentrations (MIC) of 4–166.7 μg mL^{-1}. Results for fungal strains varied in terms of their susceptibilities for the different samples tested. Zn Al Fe Co Ni was able to inhibit the biofilm formation of *S. aureus* (96.09%), *E. coli* (98.32%), and *Candida* (*C.*) *albicans* (95.93%). This study shown that certain LDH categories, particularly Zr Al Fe Co Ni, may be promising antibacterial agents against variety of pathogenic microorganisms that cause serious infections.

[a] Chemistry Department, Faculty of Science, Beni-Suef University, Beni-Suef 62511, Egypt. E-mail: radwaraft@yahoo.com; rehabkhaled@science.bsu.edu.eg; doaae4657@gmail.com

[b] Department of Materials Science and Nanotechnology, Faculty of Postgraduate Studies for Advanced Sciences, Beni-Suef University, Beni-Suef 62511, Egypt. E-mail: zienab_ryad@yahoo.com; yasser191919@gmail.com

[c] Biological Science Department, College of Science, King Faisal University, P. O. Box 400, Al-Ahsa 31982, Saudi Arabia

[d] Botany and Microbiology Department, Faculty of Science, Beni-Suef University, Beni-Suef 62511, Egypt. E-mail: akhalifa@kfu.edu.sa

[e] Department of Biology, College of Science, Princess Nourah Bint Abdulrahman University, P. O. Box 84428, Riyadh 11671, Saudi Arabia. E-mail: sialothman@pnu.edu.sa

[f] Department of Zoology, Faculty of Science, Beni-suef University, Beni-suef 65211, Egypt. E-mail: Ahmed.aliahmed@science.bsu.edu.eg

[g] Department of Pharmacology, Faculty of Veterinary Medicine, Beni-Suef University, 62511, Egypt. E-mail: Fatma.aboel3la@vet.bsu.edu.eg; fa.pharma@yahoo.com

[h] Department of Hygiene, Zoonoses and Epidemiology, Faculty of Veterinary Medicine, Beni-Suef University, Beni-Suef 62511, Egypt. E-mail: abdelaziz.sahar@yahoo.com

[i] Environmental Science and Industrial Development Department, Faculty of Postgraduate Studies for Advanced Sciences, Beni-Suef University, Beni-Suef 62511, Egypt. E-mail: amal_2006z@yahoo.com

1 Introduction

Inorganic nanomaterials have received considerable interest as promising agents for various biotechnological applications, particularly in bio-medicine. LDHs and hydrotalcite-like materials, which are anionic clays, are a category of inorganic nanosheets with structurally positively charged layers and interlayer balancing anions.[1,2] LDHs have a wide range of applications in polymer and magnetic materials industries, catalysis, biomedical and agricultural applications, and environmental remediation. LDHs are characterized by relatively high specific surface area resulting from the layered structure, the nanometric particle size, and the excellent biocompatibility and biodegradability.[3] One particular application of inorganic nanomaterials and LDH in particular that received wide interest is their use as the next generation antimicrobial agents. This is due to the emergence of the phenomenon known as antimicrobial resistance (AR), which is the development of microbial changes that lead to the antimicrobials losing their effectiveness and being no longer active against microbial pathogens.[4]

AR is one of the greatest challenges to world health and food security, causing substantial societal and economic damage. According to the World Health Organization, antimicrobial resistance is responsible for 700 000 deaths annually around the world,

posing potential health concerns. AR challenges treatments for diseases such as pneumonia, gonorrhea, and salmonellosis.[5] AR poses a significant challenge to public health and human progress, impeding our capacity to effectively address a variety of infectious diseases. The efficacy of treatments for an expanding array of health care-associated infections has diminished in several regions around the globe, mostly attributable to the escalating prevalence of antibiotic resistance among infectious agents. Nevertheless, a significant percentage of these diseases may be mitigated by the use of infection prevention and control methods. Management strategies aimed at individuals carrying multi drug-resistant organisms have traditionally been seen as a balancing act between the welfare of the general population and the personal freedom of the individuals involved. Our proposal is to re-frame the ethical matter at hand and see control measures targeting carriers as a matter of solidarity. Therefore, searching for an efficient alternative approach, notably LDHs, to combat virulent microbes is of premium importance for the battle with humans.[5]

From the chemistry point of view, LDHs are defined as 2D anionic clay materials, similar in structure to brucite, which possess the chemical formula $[M(II)_{(1-x)}M(III)_x (OH)_2]^{x+}(A^{n-})_{x/n} \cdot yH_2O$. $M(II)$ is a divalent cation such as Mg, Cu, or Co while $M(III)$ is a trivalent cation such as Al, Cr, or Fe, and A^{n-} represents the negative anions such as CO_3^{2-}, Cl^-, NO_3^-.[6] Even though LDH have shown promising antibacterial properties, most of the studied types are binary-metallic samples.[7,8] Such samples contain one divalent and one trivalent cations to preserve the layered structure. Other studies focus on ternary LDH systems where one more divalent or trivalent cation is added to the binary root.

However, multi-metallic LDH samples began to catch recent interest due to their enhanced properties and higher performance in electro-catalytic and wastewater treatment related applications.[9] Multi-metallic samples can be synthesized by using several divalent and/or trivalent cations and assess the resulting properties. In the open literature, LDH samples containing four,[10] five,[11] seven,[12] eight,[12] and up to ten elements[13,14] were reported. Unfortunately, these multi-metallic LDH samples were not considered for antimicrobial applications and their antibacterial and antifungal properties are under studied. In this work, we consider studying the antimicrobial properties of a five element (quinary) Zr Al Fe Co Ni LDH and its Al Fe Co Ni LDH quaternary and Fe Co Ni LDH tertiary roots *i.e.* its lower elements corresponding samples. This work is the first work to report the antimicrobial properties of the five element Zr Al Fe Co Ni LDH and its corresponding four and three root LDH samples. The different properties of the prepared samples were characterized using X-Ray Diffractometer (XRD), Fourier Transform Infrared (FTIR), Scanning Electron Microscope (SEM), zeta size, zeta potential, and Brunauer–Emmett–Teller (BET) techniques. Finally, their antibacterial and antifungal properties were assessed and discussed.

2 Materials and methods

2.1 Materials and reagents

Ferric nitrate nonahydrate ($Fe(NO_3)_3 \cdot 9H_2O$), zinc nitrate ($Zn(NO_3)_2 \cdot 6H_2O$), aluminum nitrate nonahydrate ($Al(NO_3)_3 \cdot 9H_2O$), cobalt nitrate hexahydrate ($Co(NO_3)_2 \cdot 6H_2O$), nickel nitrate hexahydrate ($Ni(NO_3)_2 \cdot 6H_2O$), zirconium oxychloride ($ZrOCl_2 \cdot 8H_2O$), and sodium hydroxide were purchased from Sigma-Aldrich. All solutions and experiments were prepared and conducted by suspending the nanomaterials using deionized water (DW) and sonication with the Ultrasonic Processor at 220 V/50 Hz (Model FS/000100/T). Different media types were used in this study according to the microorganism type, such as Muller Hinton broth and Muller Hinton agar for bacterial growth, while Sabarouds Dextrose Agar (SDA) and Sabarouds Dextrose Broth (SDB) were used for fungus growth using a typical or standard antifungal treatment (cyclohexamide-growing fungi and doxycycline-standard for both Gram-positive and Gram-negative bacteria).

2.2 Synthesis of LDH

Fe Co Ni LDH with a molar ratio of 1 : 2 : 2 was synthesized using a simple bottom up co-precipitation method.[15] 100 mL of DIW containing 0.20 M Co^{2+}, 0.20 M Ni^{2+}, and 0.10 M Fe^{3+} was added to a 250 mL beaker under stirring. Then, a 2 M NaOH solution was slowly dropped under continuous stirring until pH 10 was reached. The resulting suspension solution was kept overnight at room temperature with stirring to ensure the complete precipitation of Fe Co Ni LDH. The resulting suspension was centrifuged and washed several times using DIW until pH 7 was reached. Then, the formed precipitate was kept at 50 °C in an oven for 24 h until it was completely dry. Similarly, Al Fe Co Ni LDH with a molar ratio of 0.5 : 0.5 : 2 : 2 and Zr Al Fe Co Ni LDH with a molar ratio of 0.1 : 0.5 : 0.4 : 2 : 2 were prepared following a similar procedure.[15]

2.3 LDH samples characterization

The crystallinity of the prepared materials was investigated by XRD (PANalytical Empyrean, Netherlands). The crystallite size for LDH samples was determined by the Debye–Scherrer equation $D = k\lambda/(\beta \cos \theta)$, where k is a shape factor (0.9), λ is the Cu Kα radiation wavelength (1.54060 Å), β is the peak width at half maximum (in radians), and θ is Bragg's diffraction angle.[16] The functional groups were determined using FTIR spectroscopy (Bruker-Vertex 70, KBr pellet technique, Germany), from 400 to 4000 cm1 wavenumber. The morphology of the synthesized LDH samples was investigated using a field emission SEM. Particle sizes and zeta potentials were determined on a Malvern instrument (Malvern Instruments Ltd). BET-specific surface area and pore size distribution of the prepared materials were determined by N_2 adsorption isotherms using an automatic surface area analyzer (TriStar II 3020, Micromeritics, USA).

2.4 Bacterial strains and growth conditions

All fungal isolates used in this study were acquired from the Fungal Research Institute's (Doki, Giza, Cairo) reference collection, while the bacterial strains were obtained from the American Type Culture Collection (ATCC) at the Cairo Microbiology Research Center. Strains employed for phylogenetic reconstruction represented all therapeutically important Mucorales taxa for *M. indices* (CNRMA 03894). The reference standard, doxorubicin, was provided by Pharma Swede

Pharmaceutical Company, while cyclohexamide served as the standard antifungal drug. The antibacterial study used Gram-positive *B. subtilis* (ATCC 35021), *St. pneumonia* (ATCC 49619), *S. aureus* (ATCC 25913), *L. monocytogenes* (ATCC 19115), Gram-negative *E. coli* (ATCC 25922), and *H. influenza* (ATCC 49766). *Aspergillus* (*A.*) isolates from the Regional Center for Mycology and Biotechnology (RCMB) included *A. flavus* (RCMB 02783), *A. fumigatus* (RCMB 02564), and *A. niger* (RCMB 02588), *C. albicans* (RCMB 05035), mucormycosis-causing species like *M. indicus* (CNRMA 03.894), and *Penicillium notatum* (*P. notatum*, 2881). Using Muller Hinton broth (MHB) and Muller Hinton agar (MHA), several bacterial strains were cultivated for 24 hours at 37 °C in an incubator using MHA. The temperature was maintained at 25 °C for five days while SDA and SDB were used for fungus growth using a typical or standard antifungal treatment (cyclohexamide for growing fungi and doxycycline for both Gram-positive and Gram-negative bacteria). Each test tube was autoclaved in preparation for the trials.

2.5 Determination of minimum inhibitory concentration (MIC)

The antibacterial activity of Fe Co Ni, Al Fe Co Ni, and Zr Al Fe Co Ni LDH samples against the bacterial strains was assessed using the conventional broth micro-dilution method. Using Luria-Bertani (LB) broth (Sigma-Aldrich) and a final inoculum of 10^8 CFU mL^{-1} (colony forming unit per mL), the minimum inhibitory concentration (MIC) was determined. After incubating bacterial strains with successive two-fold dilutions of the relevant compound in concentrations ranging from 1000 μg mL^{-1} to 0.97 μg mL^{-1} with adjusted bacterial concentration was used to determine MIC in LB broth for 24 h. The visible turbidity of the tubes before and after incubation served as a marker for the MIC. The control contained only inoculated broth and was incubated for 24 h at 37 °C for different tested bacteria.

2.6 Determination of minimum bactericidal concentration (MBC)

Following the MIC determination of LDHs, 100 μL aliquots from every tube that had no apparent bacterial growth were seeded into LB agar plates that had not been treated with the compound. Inoculated plates were incubated for 24 hours at 37 °C. The lowest concentration of compound that recorded no obvious bacterial growth was reported as MBC.

2.7 Agar diffusion method

The antibacterial properties of the LDH samples were determined using the agar disk diffusion method. The tested bacterial strains were spread on the surface of MHA, and sterilized disks that loaded with various concentrations of LDHs (1000, 500, and 250 μg mL^{-1}) were placed on top of the agar plates. Plates were then incubated at 37 °C for 24 hours. After incubation, the diameter of the inhibition zone around each disk was estimated. For sterilizing Whatman filter paper discs (50 mm diameter), they put in glass containers at 150 °C. Then the discs impregnated in the tested materials (1000 μg mL^{-1} suspended in water), and discs were placed in triplicate on

nutrient agar plates that had been inoculated with the relevant test organism. Standard conditions of 10^8 CFU mL^{-1} were employed for the antibacterial test. Using 12 centimeter diameter Petri plates, two filter paper discs were placed in each dish. Test organisms including *St. pneumonia*, *S. aureus*, and *L. monocytogenes*, *E. coli*, *H. influenza*, and *B. subtilis*. Doxycycline was employed as a standard antibiotic against both Gram-negative and Gram-positive bacteria, while cyclohexamide was used as a standard antifungal. The inoculated plates were incubated at 37 °C for 24 hours for bacteria species while 25 °C for 5 days for fungi.

2.8 Isolation and identification of fungal strains

Fresh cultures of *A. flavus*, *A. fumigatus*, *A. nigra*, *C. albicans*, *M. indicus*, and *P. notatum* were used to produce suspensions that were plated on SDA. After the incubation period, the specimens were transferred into test tubes that were filled with 5 mL of a saline solution with a concentration of 0.9%. This transfer was performed using a needle that had been bent. To ensure the accuracy of spore counting, the final inoculum's turbidity was standardized using either a hemo-cytometer or an automated cell counter. The utilization of liquid yeast peptone glucose medium is a common practice in the cultivation of suspension cultures. The ultimate concentration of recently gathered spores was determined to be around 1.5×10 (CFU mL^{-1}).[17]

2.9 Determination of MIC for the tested fungal isolates

MICs were estimated for *M. indicus*, *A. flavus*, *A. fumigatus*, *A. niger*, and *P. notatum* using the broth micro-dilution method. On a "U" bottom 96-well micro-dilution plate, add 100 μL of SDB medium to each well. Then add 100 μL of the tested nanomaterial emulsion to the first horizontal row of wells in the plate. Concentrations of 1000 to 1.95 μg mL^{-1} were obtained using serial dilutions of two, where a 100 μL aliquot was transferred from the highest concentration well to the next well. Then 10 μL of inoculum suspension from multiple strains tested was added to each well of the plate. Each column represents a specific fungal strain. Positive control media (media containing components but no fungal strains) and negative control media were used in the presence of a common antifungal, cyclohexamide (media containing fungi but no nanomaterials). SDA plates contained 100 μL of SDA in each well, consecutively. Dilutions at different concentrations of tested LDH (1000, 500, 250, 125, 62.5, 31.25, 15.62, 7.81, 3.90, and 1.95 μg mL^{-1}). A 10 μL solution of 1.5×10^8 fungal strain per mL was injected after diluting the NP. Plates were incubated at 25 °C for 72 hours. After the appropriate incubation time, the presence or absence of growth was visually observed. The formation of cell clusters, or "buttons," in plate wells was considered MIC, defined as the lowest concentration causing visible inhibition of fungal growth.

2.10 Minimum fungicidal concentration (MFC) assay

To calculate the MFC, 10 μL aliquots of MIC, MIC 2, and MIC 4 of the tested nanomaterials, cyclohexamide, and negative controls for fungal growth were subculture onto SDA-coated

Petri dishes. Readings were taken to assess MFC based on control growth after 72 hours of incubation at 25 °C, MFC was defined as the lowest product concentration that prevented the development of various fungal species and resulted in either 50.0 or 99.9% fungicidal activity. For calculation of MIC and MFC, the experiments were presented at triplicate. While it was possible to test the efficacy of the substance using both dilution techniques, it was impossible to say whether this was the case. The chemicals kill the fungus or just stop it from growing. MFC testing is used to achieve this goal. A small aliquot of each, depending on the fungal species to be tested, broth dilution assays are sub-cultured on a rich solid medium at a pre-determined time and temperature. MFC is the minimum concentration of material without bacterial growth.[18] Additionally, MFC can provide information on bactericidal or bacteriostatic activity. If MFC equals MIC, compound fungicide, but if the MFC is higher than the MIC, it is bacteriostatic.[18]

2.11 Sorbitol assay-effect of LDH on the cell wall of different tested fungal strains

To evaluate potential pathways involved in the antifungal activity of the test nanomaterials against different fungal cell walls, assays were performed using a medium with and without sorbitol (control). The culture medium (peptone–water medium) was supplemented with sorbitol at a concentration of 0.8 M sorbitol peptone–water medium (15 g L^{-1}). Assays were performed using 96-well 'U'-shaped plates using the microdilution technique. Readings were taken on day 5 of incubation after plates were aseptically sealed and incubated at 25 °C. The higher MIC values observed in media supplemented with sorbitol compared to normal media suggested the cell wall was one of the sources of the higher MIC values, as sorbitol can act as an osmo-protectant for fungal cell walls.

2.12 Antifungal assay

LDH samples to be tested were used to detect antifungal activity using the agar dilution method. The antifungal activity of the investigated nanomaterials was determined using the methodology of Jeff-Agboola et al.[19] for several randomly selected fungal isolates. The tested fungal strains were cultured on SDA at 25 °C for 72 hours and then suspended in physiological saline (0.9% NaCl) at 1.5 × 10^8 CFUs. The tested nanomaterials were mixed with SDA during the manufacturing test concentration and autoclaved at 121 °C for 15 minutes. It is kept at 55 °C. Concentrations of 1, 2, and 3 percent of LDHs were used in a test, and 20 mL of solidified SDA was then added into a sterile Petri dish. Then, after 72 hours, the growth was observed and calculated.

2.13 Anti-biofilm potential

As described by Christensen et al.[20] a qualitative assay was performed to assess the inhibition of biofilm formation in the presence and absence of the synthesized Zn Al Fe Co Ni, Al Fe Co Ni, and Fe Co Ni LDHs. A visual examination of biofilm formation on tube walls was conducted in the absence and presence of the synthesized LDHs. The anti-biofilm activity of the synthesized LDHs (10.0 µg mL^{-1}) was examined against S. aureus and C.

albicans. It was evaluated and compared to an untreated control.[21] Briefly, 5 mL of nutrient broth (NB) was added to tubes and inoculated with 0.5 McFarland-adjusted cultures to 1–2.5 × 10^8 CFU mL^{-1}. After 24 h of incubation at 37.0 ± 0.5 °C, the contents were discarded, washed with PBS (pH = 7.0), and dried. The bacterial and yeast cells adhered to the tube walls were fixed with 5 mL of 3.0% sodium acetate for 15 minutes and rinsed with deionized water. The biofilms were stained with 0.1% crystal violet (CV) dye for 15 minutes and washed to remove excess of the dye. For semi-quantitative anti-biofilm estimation, 5 mL of absolute ethanol was added to dissolve the CV-stained biofilms. The optical density (OD) of the dissolved biofilms was measured by Ultraviolet-visible (UV-Vis) spectrophotometry at 570 nm.[22] The biofilm inhibition percentage was calculated the eqn (1);[23]

$$\text{Biofilm inhibition\%} = [\text{OD of control sample} - \text{OD of treated sample}/\text{OD of control sample}] \times 100 \quad (1)$$

2.14 Growth curve assay

To evaluate the effect of the synthesized Zn Al Fe Co Ni, Al Fe Co Ni, and Fe Co Ni LDHs on the S. aureus kinetic growth curve, the method of Huang et al.[24] was conducted. First, the bacterial inoculum was standardized to 0.5 McFarland (2 × 10^8 CFU mL^{-1}). The synthesized Zn Al Fe Co Ni, Al Fe Co Ni, and Fe Co Ni LDHs were mixed into tubes containing S. aureus. The OD at 600 nm wavelength was measured every 2 hours for 24 hours. The average of duplicate readings was plotted against time (hours) to construct the standard growth curve and assess the impact of the LDH samples on S. aureus growth kinetics.[25]

2.15 Effect of UV illumination on the antimicrobial and antifungal activity

tThe antimicrobial potential of the synthesized Zn Al Fe Co Ni, Al Fe Co Ni, and Fe Co Ni LDHs with and without UV illumination was assessed against the most sensitive S. aureus and C. albicans using the optical density method.[26] The tested microbes were stimulated in nutrient broth (NB) overnight at 37 °C. Firstly, 0.5 mL of the overnight culture were inoculated into 5 mL NB tubes that were adjusted after 2 hour of incubation to the standard 0.5 McFarland concentration (2 × 10^8 CFU mL^{-1}) and 0.400 (1 × 10^4 cells per mL) of C. albicans. 100 µL of synthesized Zn Al Fe Co Ni, Al Fe Co Ni, and Fe Co Ni LDHs were mixed into the tubes and then incubated at 37 °C for 60 min. The mixture tubes were divided into two conditions: with and without UV illumination. While tubes without synthesized Zn Al Fe Co Ni, Al Fe Co Ni, and Fe Co Ni LDHs were inoculated with bacteria and fungi and used as the positive control (subject to UV), tubes without UV illumination were used as the negative control. They were exposed to UV light for various time periods (0, 15, 30, 45, and 60 minutes). Turbidity was noted to form in the treated samples and was measured at a specific wavelength (600 nm for bacteria and 630 nm for fungi). Typically, the UV lamp (7.0 mW cm2) was fixed over the samples at 37 °C. were displayed at various times (0, 15, 30, 45, and 60 min) at 37 °C with an intensity of 7.0 mW cm^{-2} disturbance on the individuals and the turbidity of the samples,

the inhibition percentage of the examined bacterial pathogens was determined by equation.[27]

2.16 Protein leakage assay

To determine the potential antibacterial mechanism of the synthesized Zr Al Fe Co Ni, Al Fe Co Ni, and Fe Co Ni LDH samples, a protein leakage assay was performed. Bacterial inocula were standardized to 0.5 McFarland (2×10^8 CFU mL^{-1}) and mixed with varying concentrations of the LDH nanoparticles. Cultures without LDHs were used as negative controls. After incubating at 37 °C for ~5 hours, the samples were centrifuged at 5000 rpm (round per minute) for 20 minutes to separate bacteria from the supernatant. 100 μL of collected supernatants were mixed with 1 mL of Bradford reagent, and absorbance was measured at 600 nm after 10 minutes of incubation at 37 °C.[28]

2.17 Statistical analysis

The data were analyzed by ANOVA using descriptive statistics including mean and standard deviation. Tukey's *post hoc* test was done for the analysis of MBC and MBC. The significance of all the statistical tests was predetermined at $P < 0.05$.

3 Results

3.1 LDH samples characterization

FTIR spectroscopy analysis was carried out for all the prepared samples as shown in Fig. 1a. As illustrated, all the prepared samples showed similar peak patterns, which is expected due to the similarity of structure between the LDH roots and the higher member quinary LDH sample. The peak at 766 cm^{-1} is characteristic band of M − O bond of the LDH related to the brucite like structure where M represents a metal cation *e.g.* Fe^{3+}, Co^{2+}, Ni^{2+}, Al^{3+}, or Zr^{2+}.[29] The band observed at 1635 cm^{-1} and 1370 cm^{-1} can be attributed to –OH bending vibrations[30] and the ν_3 stretching vibration of the nitrate groups in the interlayer of LDH,[31] respectively. The peaks at 3425 cm^{-1} can be ascribed to the OH stretching vibration and bending, respectively.[32]

XRD pattern of Fe Co Ni, Al Fe Co Ni, and Zr Al Fe Co Ni LDH samples is displayed in Fig. 1b. As shown, all samples showed
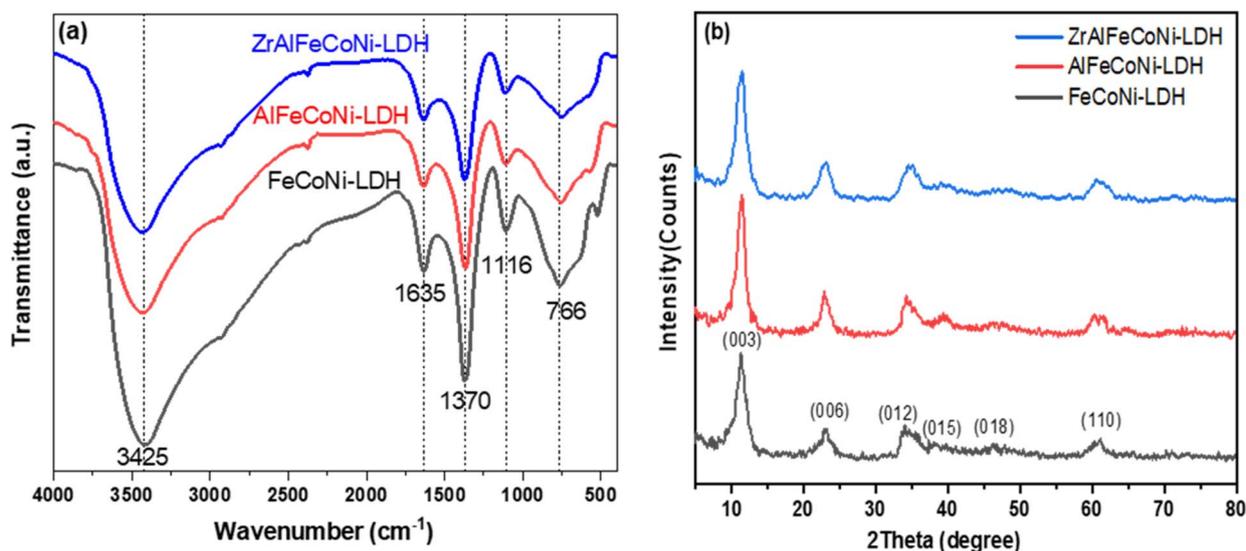

Fig. 1 FTIR (a) and XRD (b) of the tested Fe Co Ni LDH, Al Fe Co Ni LDH and Zr Al Fe Co Ni LDH.
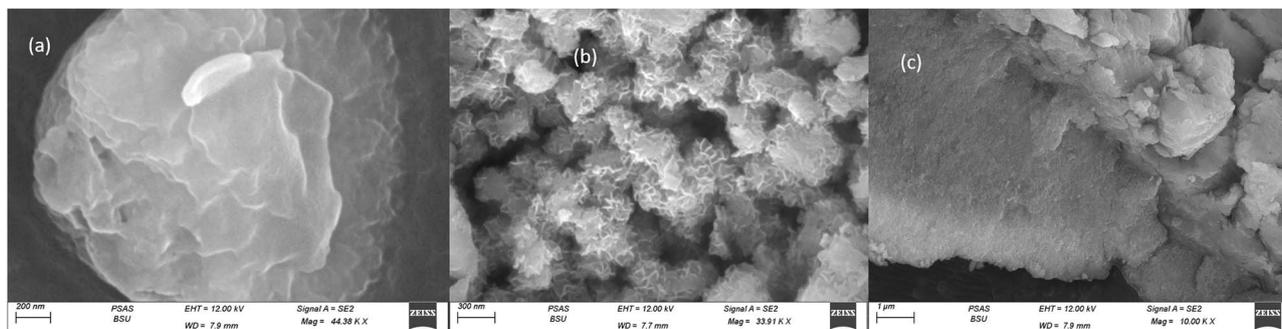

Fig. 2 SEM images of the tested Fe Co Ni LDH (a), Al Fe Co Ni LDH (b), and Zr Al Fe Co Ni LDH (c).

typical XRD peaks of the brucite like structure. The diffraction peaks at diffraction peaks at 11.3°, 22.8°, 34.3°, 39.5°, 46.2°, and 61° can be attributed to 003, 006, 012, 015, 018, and 110 planes, respectively.[33] The crystallite size for LDH samples was determined by Debye–Scherrer equation and was calculated to be 3.98, 4.88, and 4.2 nm for Fe Co Ni and Al Fe Co Ni and Zr Al Fe Co Ni LDH, respectively. The (003) interlayer distance was calculated to be 7.79, 7.72, and 7.81 Å for the Fe Co Ni LDH, Al Fe Co Ni, LDH, and Zr Al Fe Co Ni LDH respectively. These values showed no significant variation because for all samples no intercalating organic compound was used that may alter such interlayer distance if it was inserted between the LDH layers.

Fig. 2 illustrated the morphology of the prepared LDH samples. As shown, all samples were formed in an aggregated, layered structure. These layers were the typical morphology of such LDH samples prepared without the utilization of any structure-directing agents. The extensive aggregation observable in the SEM images could be attributed to the lack of surface charge in the prepared samples. This was indicated by the measurement of zeta potential, which showed values insignificantly different from zero mV for all samples, as shown in Fig. 3. This aggregation was also revealed by the measurement of hydrodynamic size, which is presented in Fig. 4. As shown, the three samples showed a very close average hydrodynamic size of approximately 300 nm. The aggregation of the LDH layers was thought to be mainly influenced by the lack of surface charge, as indicated by the zeta potential measurements.

Fig. 5a showed the nitrogen adsorption–desorption isotherms of the prepared samples. According to the IUPAC
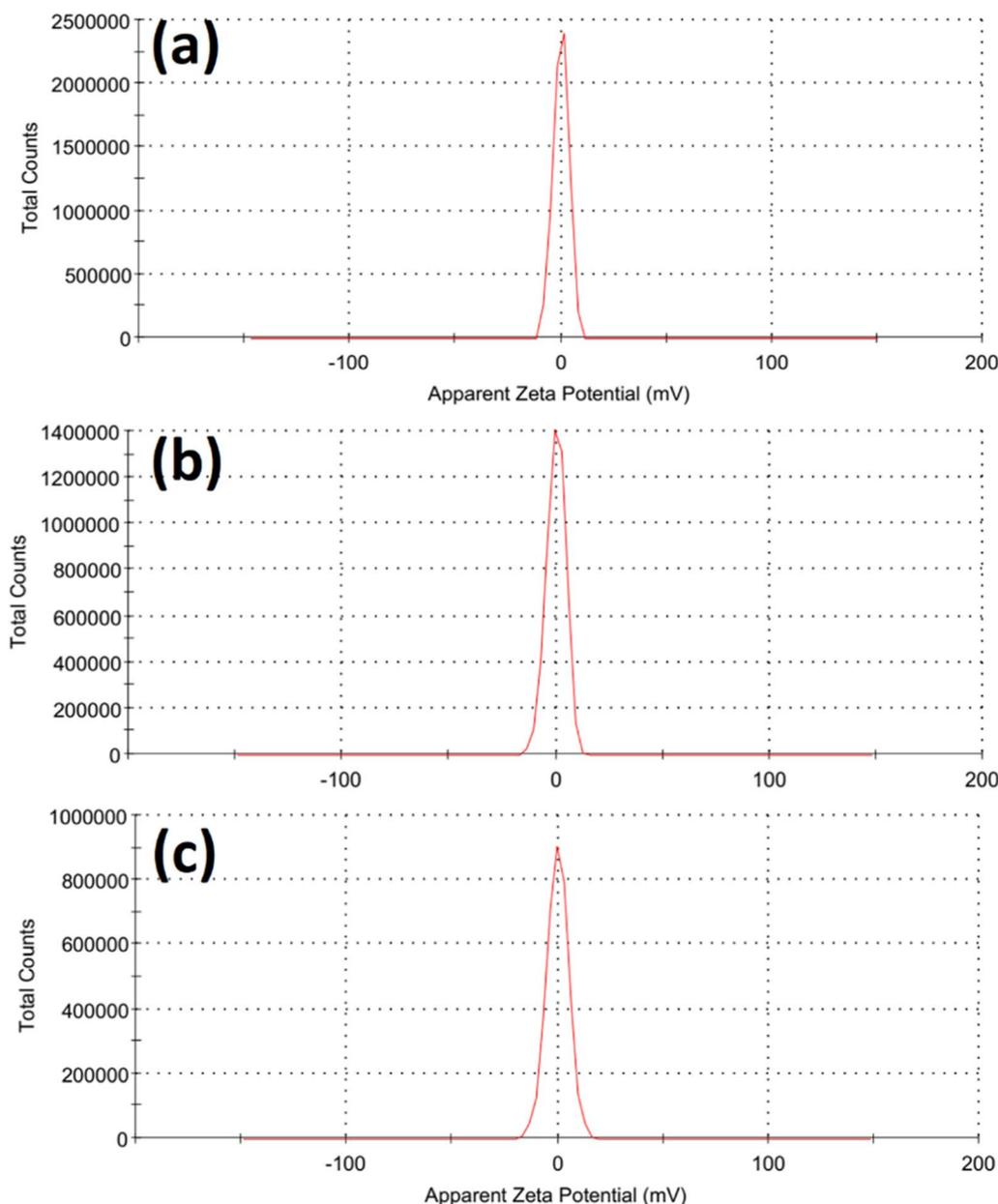

Fig. 3 Zeta potential of the tested Fe Co Ni LDH (a), Al Fe Co Ni LDH (b), and Zr Al Fe Co Ni LDH (c).
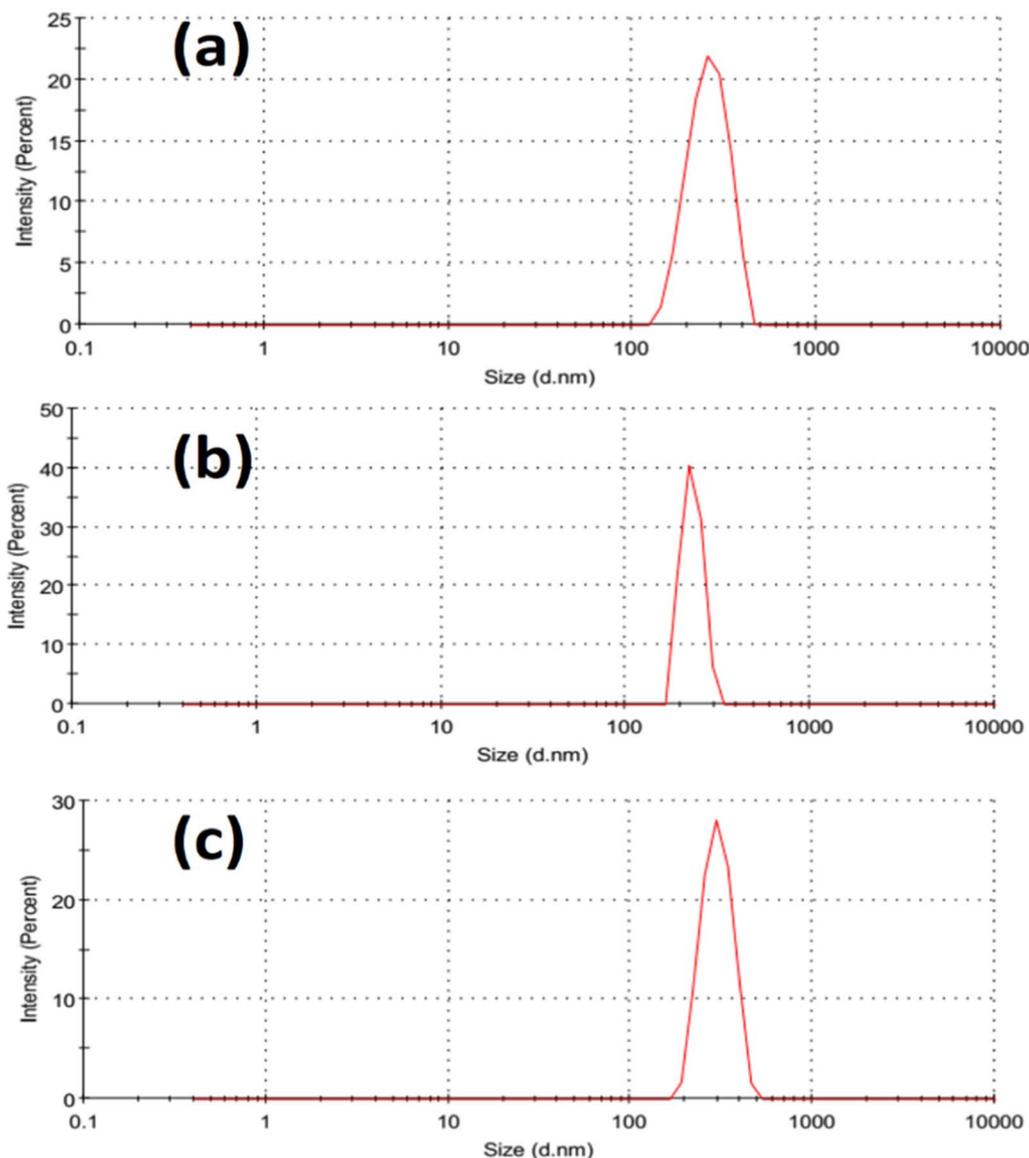
Fig. 4 Hydrodynamic size of the tested Fe Co Ni LDH (a), Al Fe Co Ni LDH (b), and Zr Al Fe Co Ni LDH (c).

classification, all samples showed an isotherm that could be classified as type IV adsorption isotherm that indicated the presence of mesoporosity in all the samples.[34] Fe Co Ni LDH and Zr Al Fe Co Ni LDH showed an H3 hysteresis loop produced from slit shaped pores, which is a typical behavior for layered 2D nanomaterials. On the other hand, Al Fe Co Ni LDH showed an H2(b) loop that reflects pore-blocking/percolation in a relatively narrow range of pore necks.[34] This may be caused by the observable low average pore size of 7 nm, as shown in Fig. 5b and Table 1, as compared to 17 nm and 13 nm for Fe Co Ni LDH and Zr Al Fe Co Ni LDH, respectively.

As illustrated in Table 1, the surface area of Al Fe Co Ni LDH showed a remarkable value of 143.25 $m^2 g^{-1}$ as opposed to 26.2 $m^2 g^{-1}$ and 45.4 $m^2 g^{-1}$ for Fe Co Ni LDH and Zr Al Fe Co Ni LDH, respectively. Al Fe Co Ni LDH showed also a high total pore volume and mono-layer capacity values of 0.426 $cm^3 g^{-1}$

and 32.91 cm^3(STP) g^{-1} respectively compared to the other two samples.

3.2 Antibacterial study

3.2.1 Determination of MIC. The values of the MIC of Fe Co Ni, Al Fe Co Ni, and Zr Al Fe Co Ni were presented in Fig. 6. As shown, the MIC of Fe Co Ni (6–500 μg mL^{-1}), Al Fe Co Ni (6.7–333.3 μg mL^{-1}), and Zr Al Fe Co Ni (4–66.7 μg mL^{-1}). It was found that Fe Co Ni, and Zr Al Fe Co Ni exhibited a comparable MIC values, whereas Zr Al Fe Co Ni displayed the most significant antibacterial activity against the tested bacterial strains as indicated by the lowest values of the MIC (4–166.7 μg mL^{-1}) (Fig. 6). Also, *E. coli* was the most resistant species as evidenced by its highest values of the MIC to Fe Co Ni, Al Fe Co Ni, and Zr Al Fe Co Ni. *E coli* had MIC values; 500 and 166.7 μg mL^{-1} for Fe Co Ni and Zr Al Fe Co Ni, respectively. On contrary, *S. aureus* was
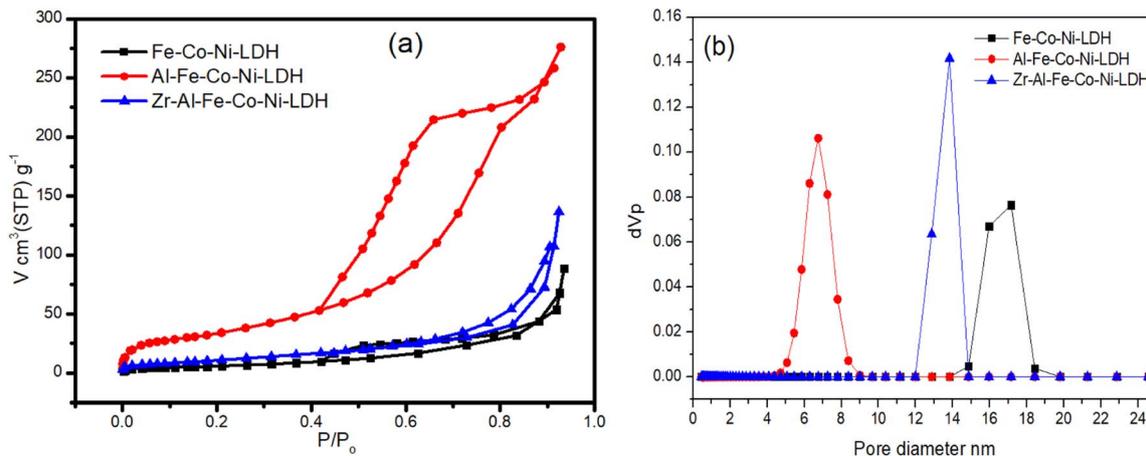
Fig. 5   Nitrogen adsorption–desorption isotherms (a) and pore size distribution (b) of the tested Fe Co Ni LDH, Al Fe Co Ni LDH, and Zr Al Fe Co Ni LDH.

Table 1   Surface area, pore volume, mono-layer capacity, and average pore diameter of the synthesized samples

	Fe Co Ni LDH	Al Fe Co Ni LDH	Zr Al Fe Co Ni LDH
Surface area ($m^2\ g^{-1}$)	26.2	143.25	45.4
Total pore volume ($cm^3\ g^{-1}$)	0.136	0.426	0.211
The monolayer capacity (cm^3 (STP) g^{-1})	6.02	32.91	10.43
Average pore diameter (nm)	17	7	13
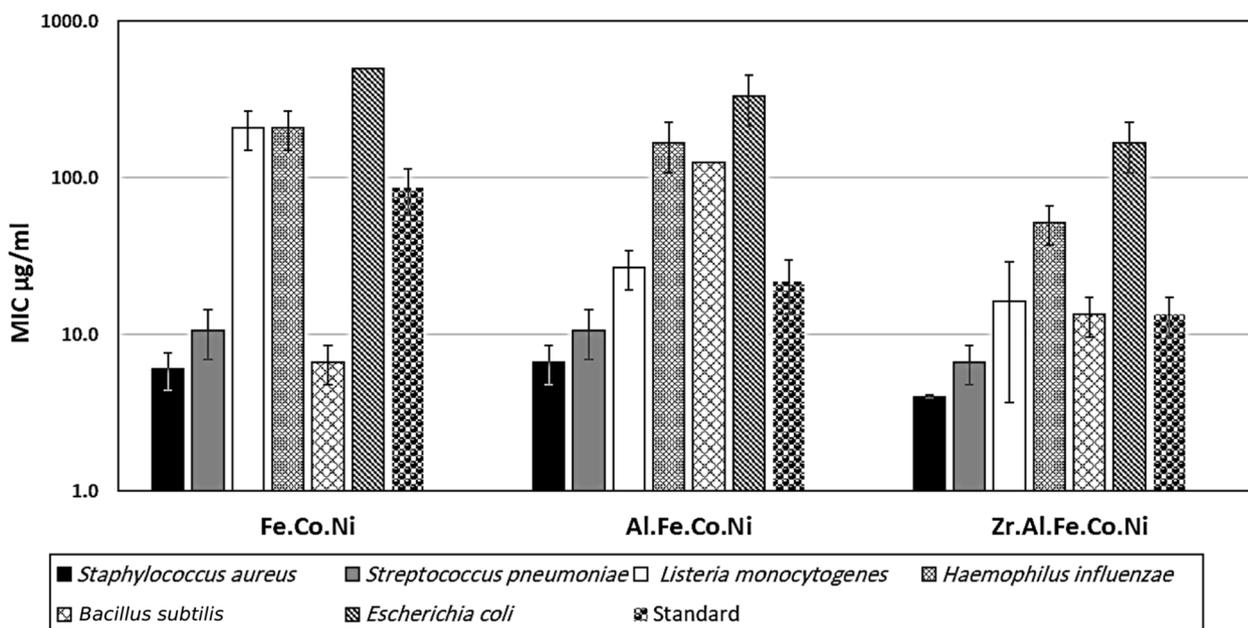
Fig. 6   Minimum inhibitory concentrations of Fe Co Ni, Al Fe Co Ni, Zr Al Fe Co Ni LDHs, and doxycycline against the tested bacterial strains.

inhibited/killed by the lowest concentrations of Fe Co Ni, Al Fe Co Ni and Zr Al Fe Co Ni (Fig. 6).

    3.2.2 Determination of MBC. Fig. 7 presented the minimum bactericidal concentration patterns. The MBCs of Fe Co Ni, Al Fe Co Ni, and Zr Al Fe Co Ni were 6–500 µg mL^{-1}, 13.3–

500 µg mL^{-1}, and 4–166.7 µg mL^{-1}, respectively. For the three LDHs, Zr Al Fe Co Ni displayed the most potent and bactericidal activity against the bacterial strains, as revealed by the MBC values (4–166.7 µg mL^{-1}) (Fig. 5). Among the tested bacterial strains, *E. coli* was the most resistant species, as demonstrated
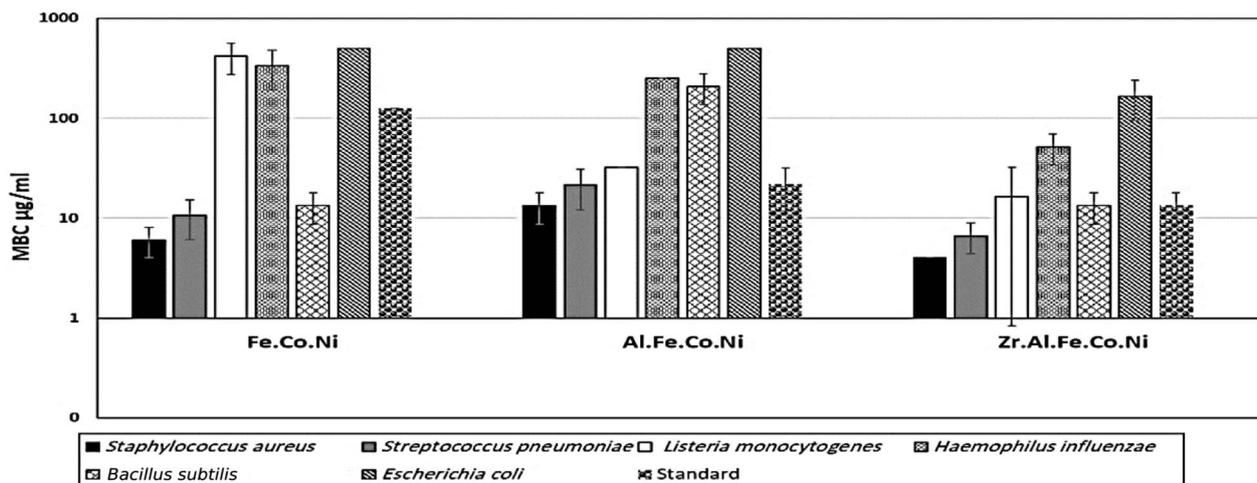
Fig. 7 MBCs of Fe Co Ni, Al Fe Co Ni and Zr Al Fe Co Ni against the tested bacterial strains with doxycycline standard drug.

by the highest and similar MBC value (500 µg mL^{-1}) to Fe Co Ni and Al Fe Co Ni. On the other hand, *S. aureus* was inhibited or killed by the lowest concentrations of Fe Co Ni, Al Fe Co Ni, and Zr Al Fe Co Ni, indicating its high susceptibility toward the LDHs tested (Fig. 7). Unlike Al Fe Co Ni, both Fe Co Ni and Zr Al Fe Co Ni exhibited a comparable MIC and MBC pattern.

3.2.3 Zone of inhibition. The antibacterial activity of Fe Co Ni, Al Fe Co Ni, and Zr Al Fe Co Ni LDHs against the six bacterial strains resulted in the formation of zones of inhibition of variable diameters (13–31 mm, 13.3–32 mm, and 13.3–32.33, respectively) (Fig. 8A and C). The diameter of the zone of inhibition increased with increasing concentrations of Fe Co Ni, Al Fe Co Ni, and Zr Al Fe Co Ni, Zr Al Fe Co Ni (1000) resulting in the greatest diameter (32.33 mm), which was reported against *S. aureus* and *St. pneumonia*. Both bacterial strains exhibited comparable susceptibility patterns toward the compounds tested at the varying concentrations examined (1000, 500, 250, and 125 µg). A similar result was noticed for *L. monocytogenes* and *H. influenza*. Additionally, the diameter of the zones of inhibition developed around *S. aureus* and *St. pneumonia* was significantly larger than that of the standard under all conditions tested.

3.3 Antifungal study

3.3.1 MIC assay. When defining standard testing criteria for an antimicrobial susceptibility test, the critical factors are the reproducibility of susceptibility endpoints and the detection of *in vitro* resistance. The MIC values of Fe Co Ni, Al Fe Co Ni, and Zr Al Fe Co Ni compounds against six fungal species: *A. flavus*, *A. fumigatus*, *A. niger*, *Mucor* sp., *P. notatum* and *C. albicans* on SDB were presented (Fig. 9). Al Fe Co Ni showed the highest MIC value against *A. flavus* (416 µg mL^{-1}), whereas the lowest MIC value was reported for Zr Al Fe Co Ni against *Mucor* sp. (21 µg mL^{-1}). Fe Co Ni displayed an MIC range of 31 µg mL^{-1} for *Mucor* sp. To 333 µg mL^{-1} for *A. flavus*. The fungal strains varied in their susceptibilities toward the different compounds tested.

Generally, in the presence of sorbitol, the MIC values were significantly lower than those in the absence of sorbitol. MIC values (in the presence of sorbitol) ranged from 10.6 µg mL^{-1} for Zr Al Fe Co Ni against *Mucor* sp. To 10.6 µg mL^{-1} for Fe Co Ni against *A. flavus*. However, Fe Co Ni and Al Fe Co Ni resulted in similar MIC values (62 µg mL^{-1} and 31 µg mL^{-1}, respectively) against *P. notatum* in the presence and absence of sorbitol. *A. niger* and *A. fumigatus* displayed an identical susceptibility to Fe Co Ni and Al Fe Co Ni, as evidenced by the same MICs (125 µg mL^{-1} and 166.6 µg mL^{-1}, respectively).

3.3.2 MFC assay. The MFCs of Fe Co Ni, Al Fe Co Ni, and Zr Al Fe Co Ni compounds against six fungal species range from 16 µg mL^{-1} for Zr Al Fe Co Ni against *M. indicus* to 500 µg mL^{-1} for Fe Co Ni against *A. flavus* (Fig. 10). These results are substantially lower than those reported in the presence of sorbitol (Fig. 8). Zr Al Fe Co Ni was the most potent antifungal agent, followed by Al Fe Co Ni and then Fe Co Ni, as indicated by the MFCs in the presence and absence of sorbitol. *A. flavus* exhibited high resistance to Al Fe Co Ni (MFC was 500 µg mL^{-1}) compared to the other compounds.

3.3.3 Zone of inhibition. The antimicrobial activities of Fe Co Ni, Al Fe Co Ni, and Zr Al Fe Co Ni on the six fungal strains resulted in the formation of zones of inhibition with variable diameters (Fig. 11). It can be noticed that as the concentration of Fe Co Ni, Al Fe Co Ni, and Zr Al Fe Co Ni increased, so did the diameter of the zone of inhibition. Fe Co Ni (1000 µg) formed zones of inhibition with a similar diameter (33 mm) against *Mucor* sp. and *P. notatum* (~22 mm) against the rest of fungal strains tested (Fig. 12). Comparable patterns were obtained with Fe Co Ni (500 µg) and Fe Co Ni (250). Al Fe Co Ni (1000). *Mucor* sp. and *C. albicans* showed a higher susceptibility to Al Fe Co Ni (1000 µg) than the remaining fungal strains examined. Zr Al Fe Co Ni (1000 µg) resulted in the formation of zones of inhibition with a similar diameter (33 mm) against *M. indicus* and *P. notatum* (~22 mm) against the rest of the fungal strains tested.

3.3.4 Percentage of inhibition. Fe Co Ni, Al Fe Co Ni, and Zr Al Fe Co Ni were mostly inhibitory to the growth of the fungi, with the percentage of inhibition ranging from 60.0% for Al Fe
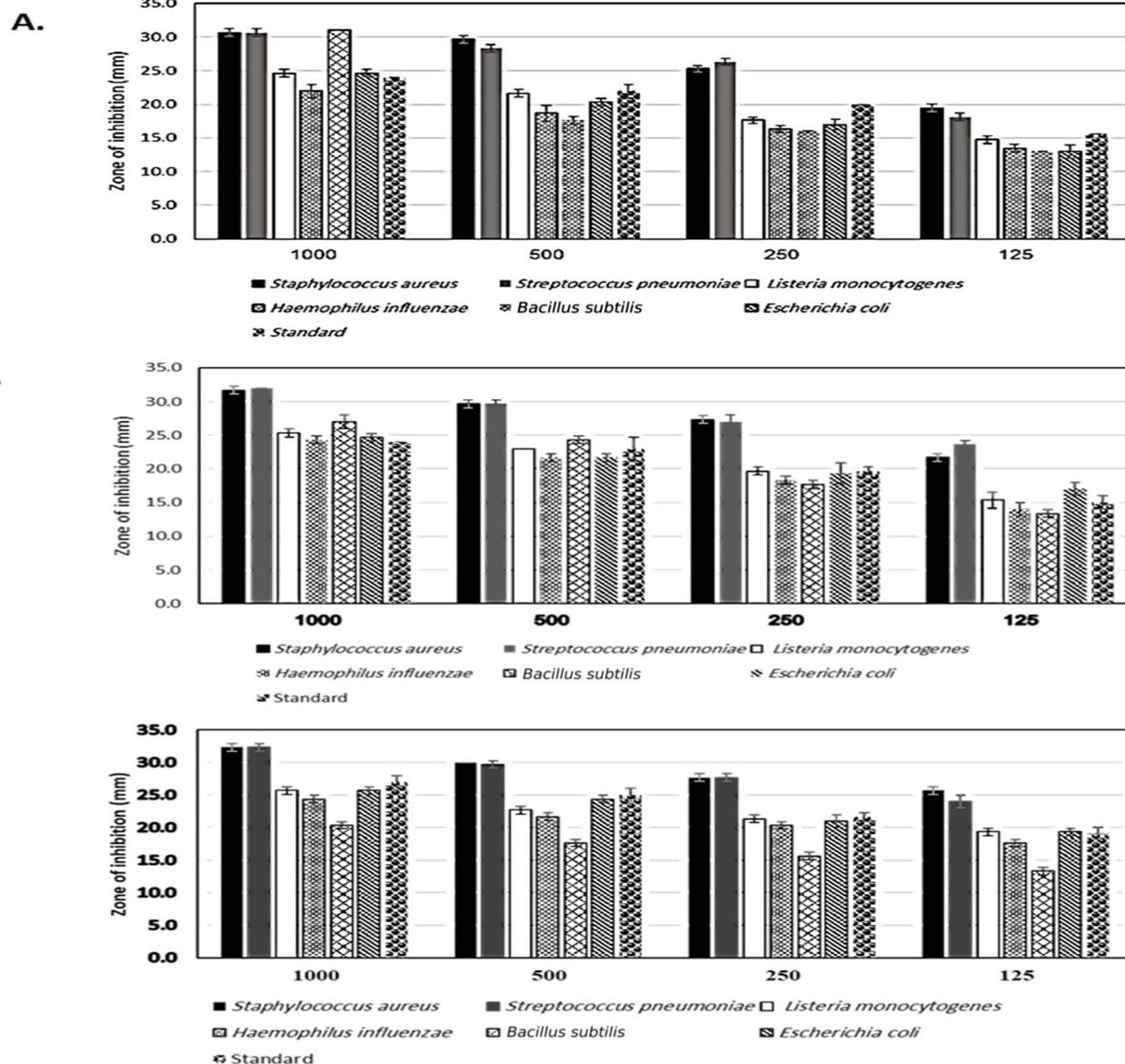
Fig. 8 Zone of inhibition developed by various concentrations (1000, 500, 250, and 125 μg) of Fe Co Ni (A), Al Fe Co Ni (B), and Zr Al Fe Co Ni (C) against bacterial strains in presence of doxycycline standard drug. As shown; zone of inhibition increased in Zr Al Fe Co Ni (C) when compared to (A) and (B) which confirm the increasing antimicrobial activity by adding Zr.

Co Ni against *A. niger* to 97.0% for Zr Al Fe Co Ni against *Mucor* sp. Similarly, Fe Co Ni showed higher activity against *M. indicus* (87.0%) and *P. notatum* (80.0%) than that against *A. niger* (60.0%) and *A. flavus* (65.0%) (Fig. 13). Among the fungal strains investigated, *Mucor* sp. was the most susceptible organism to the three compounds.

3.4 Anti-biofilm potential treatment

Certain pathogenic microorganisms are identified for the development of biofilm through production of exopolysaccharide molecules.[35] The tube method was utilized to evaluate the anti biofilm potential of the synthesized Zr Al Fe Co Ni, Al Fe Co Ni, and Fe Co Ni LDHs against some pathogenic bacteria and fungi.[36] The tube assay steps were showed Table 2.

First, normal microbial growth and ring formation in control tubes without LDHs, indicating biofilm development. Inhibited growth in tubes with LDHs showed the prevention of biofilm. To follow, the established biofilm it stained with CV dye for visual and qualitative measurement. Finally, the CV stain was extracted from adhered cells using ethanol for semi-quantitative assessment of biofilm inhibition percentage (Table 2). The tube design evaluates the anti biofilm potential of Zr Al Fe Co Ni, Al Fe Co Ni, and Fe Co Ni LDHs against bacteria and fungi. A thick whitish-yellow layer at the air–liquid interface indicates biofilm formation in LDHs (control tubes). The adhered layers stain blue with CV. A dark blue color develops when CV is dissolved in ethanol. Additionally, bacterial ring development was limited, and the anti biofilm results of the synthesized Zr Al Fe
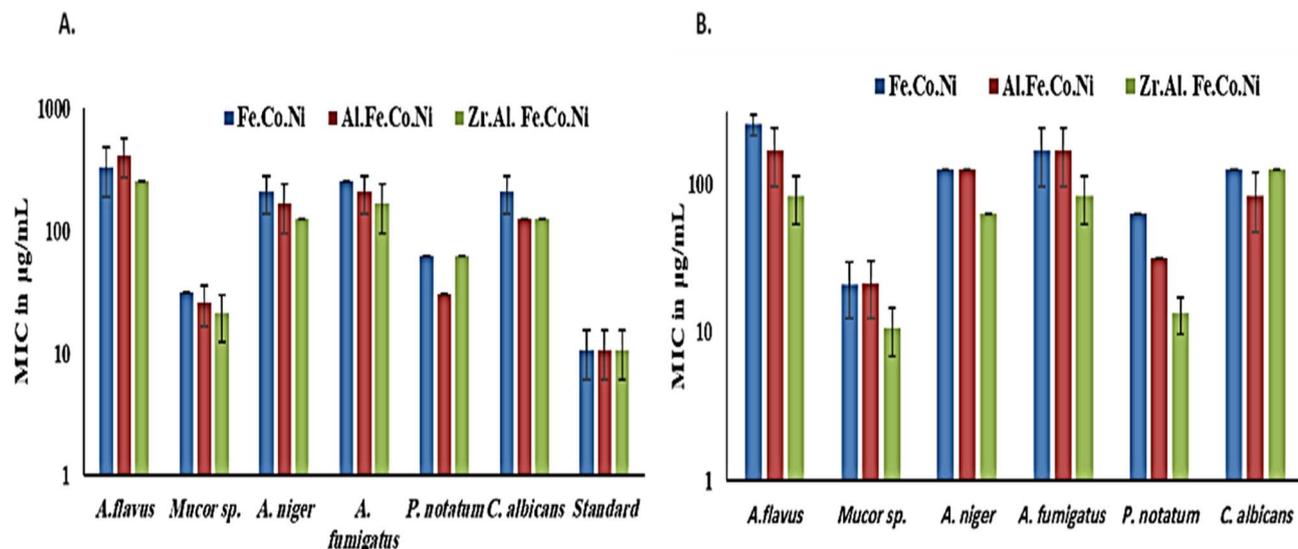
Fig. 9 MIC of Fe Co Ni, Al Fe Co Ni, and Zr Al Fe Co Ni against fungal species, (A) in normal medium and (B) in presence of sorbitol with cyclohexamide as standard drug. At the MIC; the lowest concentration was capable of showing visible antimicrobial and antifungal activity was Zr–Al Fe Co Ni better than other products.
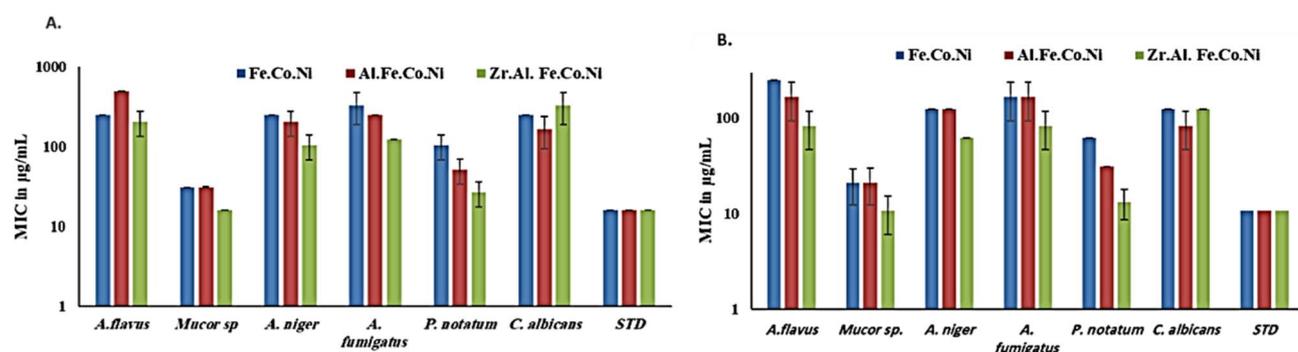

Fig. 10 MFC of Fe Co Ni, Al Fe Co Ni, and Zr Al Fe Co Ni against fungal species, (A) in normal medium and (B) in presence of sorbitol with cyclohexamide standard drug. Zr Al Fe Co Ni showed good antifungal activity in a way with higher efficacy than antibacterial activity in comparison to other structures even it also better than both Fe Co Ni and Al Fe Co Ni.

Co Ni were greater than the activity of Al Fe Co Ni and Fe Co Ni LDHs. UV-Vis spectrophotometry was used for semi-quantitative measurement of the biofilm inhibition percentage. OD was measured at 570 nm after solubilizing the crystal violet-stained biofilms. The OD570 reading correlated with the amount of stained biofilm formed, which indicated the extent of biofilm production. Table 2 showed the biofilm inhibition percentage after the addition of 10 μg mL^{-1} of each Zr Al Fe Co Ni, Al Fe Co Ni, and Fe Co Ni LDHs. The highest inhibition was seen against *S. aureus* (95.13%), followed by *St. pneumoniae*. Also, Fig. 14 showed the anti-biofilm activity of Zr Al Fe Co Ni, Al Fe Co Ni, and Fe Co Ni LDHs as percent inhibition against various pathogenic microorganisms.

3.5 Growth curve assay (kinetic study)

Fig. 15 showed the effect of synthesized Zr Al Fe Co Ni, Al Fe Co Ni, and Fe Co Ni LDHs on the growth kinetics of *S. aureus*. The

untreated *S. aureus* control displayed normal growth, reaching an OD600 of 2.00. Al Fe Co Ni and Fe Co Ni LDHs showed some inhibition, reducing the OD600 to 0.77 and 1.11, respectively. Importantly, Zr Al Fe Co Ni demonstrated a notable effect on the growth curve, decreasing the OD600 to 0.49. This indicated promising inhibition of *S. aureus* growth. Zr Al Fe Co Ni showed additionally repressing potential more than Al Fe Co Ni and Fe Co Ni LDHs.

3.6 Effect of UV illumination on the antimicrobial and antifungal potential of the synthesized materials

Fig. 16 demonstrated the comparison between the bacterial and fungal activity of *S. aureus* and *C. albicans* upon the use of synthesized Zr Al Fe Co Ni, Al Fe Co Ni, and Fe Co Ni LDHs. Under UV irradiation, bacterial and fungal growth was lowest due to the enhancement of photo-activation of LDHs. UV presentation was chosen to increase the potential for photo-
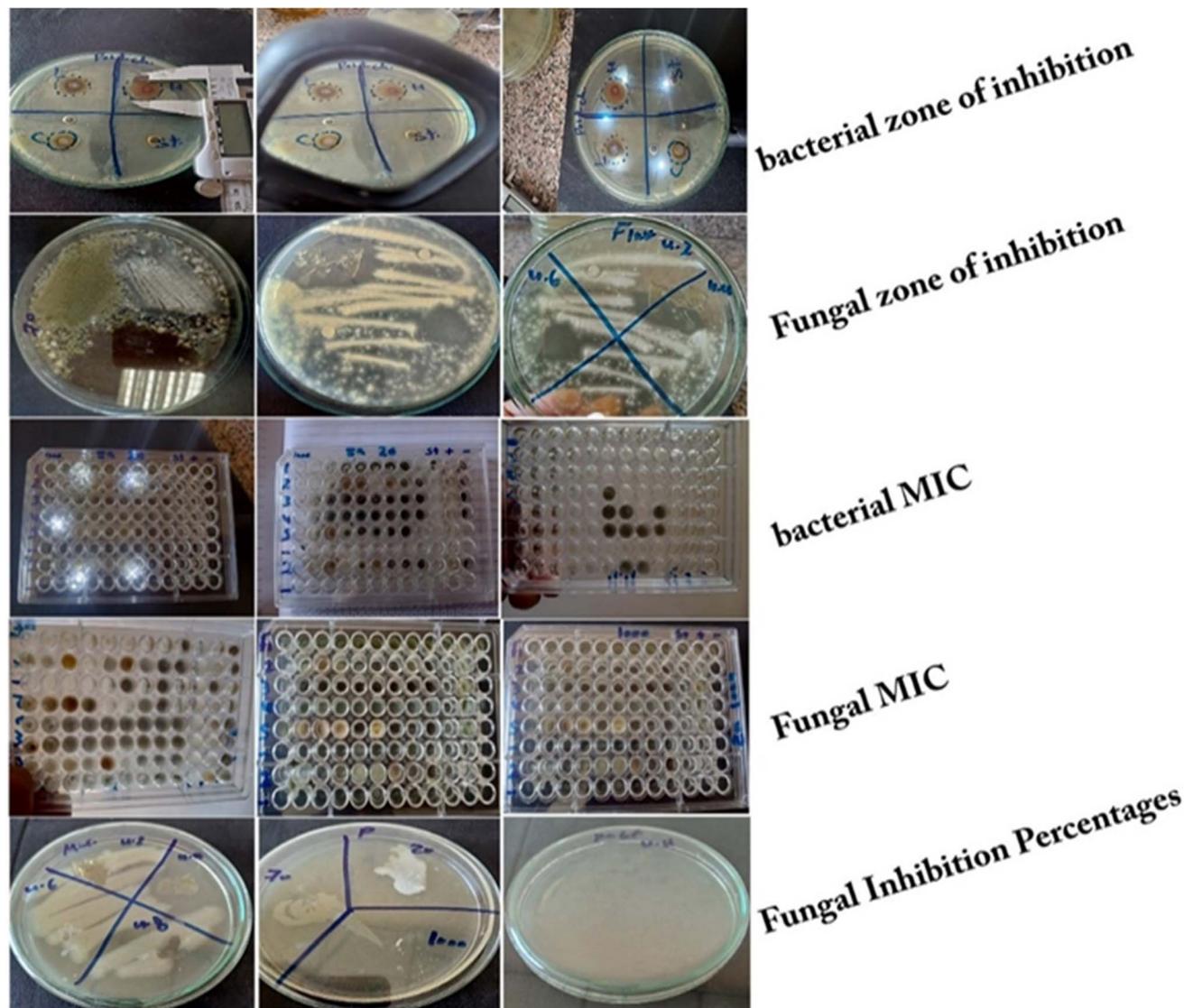
Fig. 11 Antimicrobial activity and zone of inhibition of the tested nanomaterials, where Zr Al Fe Co Ni showed the largest zone of inhibition in compared to other tested materials, percent of inhibition (%), of LDHs in SDA media against different fungal isolates *M. indicus*, *P. notatum*, *A. flavus*, *A. fumigatus*, and *A. niger* after 72 hours incubation at 25 °C for 3 days, the Zr Al Fe Co Ni showed complete fungal inhibition growth in comparison to other material where appear of fungal colonies on plates, while bacterial species at 37 °C/24 hours, measured as mean ± SD on MHA. Besides the shape of the different tested fungal isolates with 100% and zero growth the shape of the MIC (broth dilution test) at antifungal investigations.

activation of LDHs. Zr Al Fe Co Ni LDH exhibited even higher photo-catalytic potential than both Al Fe Co Ni and Fe Co Ni LDHs. The UV assay results showed that bacterial and fungal growth was significantly increased after UV illumination of Zr Al Fe Co Ni LDH compared to the non-treated control and Al Fe Co Ni and Fe Co Ni LDHs. This indicated that the incorporation of Zr into Al Fe Co Ni nanoparticles counters the inherent antibacterial property of Al Fe Co Ni UV activation.

3.7 Determination of protein leakage from bacterial cell membranes

In the protein leakage assay, cell-free bacterial supernatant were used to quantify the amount of protein released from the bacterial cells. As shown in Fig. 17, the quantity of leaked bacterial proteins increased proportionally with higher concentrations of the synthesized LDHs. At 1.0 mg mL^{-1} concentration, the protein content released was 191.98 μg mL^{-1} for Zr Al Fe Co Ni LDH and 141.3 μg mL^{-1} and 124.88 μg mL^{-1} for Al Fe Co Ni and Fe Co Ni LDHs, respectively. These results demonstrate the enhanced antibacterial effect of Zr Al Fe Co Ni LDH, confirming its catalytic antibacterial activity. Zr Al Fe Co Ni LDH was observed to accumulate around *S. aureus* cells and membrane, indicating leakage of protein molecules from the *S. aureus* membrane and confirming their presence in the bacterial cytoplasm.
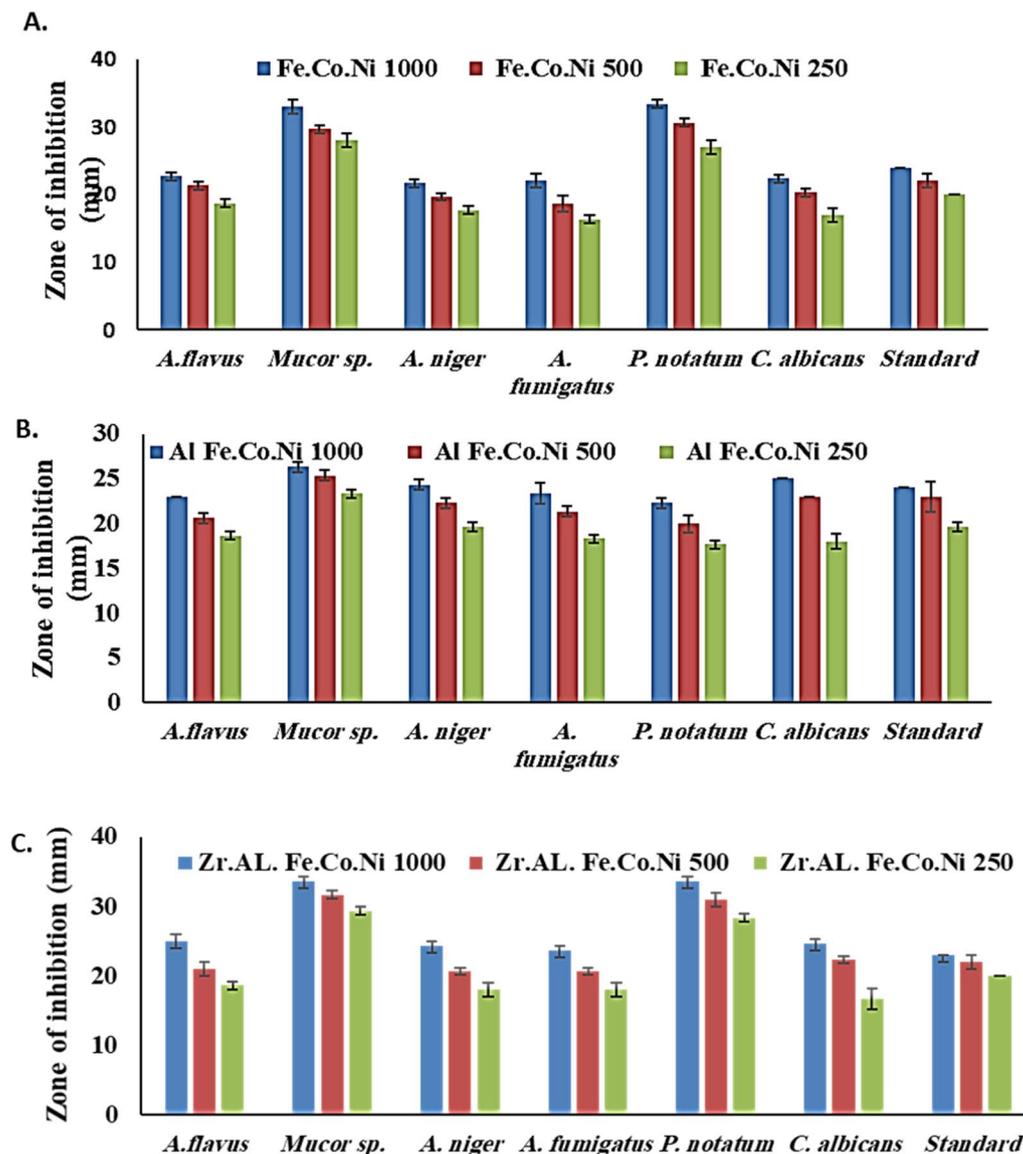
Fig. 12 Zone of inhibition developed by various concentrations (1000, 500, 250, and 125 μg) of Fe Co Ni (A), Al Fe Co Ni (B), and Zr Al Fe Co Ni (C) against fungal strains with cyclohexamide standard drug. The highest antifungal activity showed by Zr Al Fe Co Ni especially against *M. indicus* indicating the higher efficacy of the Zr Al Fe Co Ni as antifungal agent.

4 Discussion

Multi-metallic LDH have gained wide interest recently due to their enhanced properties and wide range of possible applications.[9] Studies usually focus on two-element LDH samples where one divalent and one trivalent cation are used. However, increasing the number of any of these cations can lead to the formation of multi-metallic LDH samples, which may show enhanced performance and improved characteristics. For instance, the introduction of a third cation, thereby forming a ternary LDH, was reported to enhance the properties of the synthesized samples for electro-catalytic and wastewater treatment applications.[9] Beyond ternary LDH, previous studies have also reported improved performance of LDH samples with a higher number of elements, as discussed earlier in the

introduction section. In this work, ternary, quaternary, and quinary Fe Co Ni LDH, Al Fe Co Ni LDH, and Zr Al Fe Co Ni LDH were prepared using a simple co-precipitation method to explore the possible improved antimicrobial properties of multi-metallic LDH samples. As reported in the results section, the prepared samples showed similar properties in terms of crystalline size, inter-layer *d*-spacing, morphology, zeta potential, and hydrodynamic size. However, the BET surface area for the quaternary Al Fe Co Ni LDH was significantly higher than the other two samples, which represents a 5.4 and 3.1 fold increase compared to that of the Fe Co Ni LDH and the Zr Al Fe Co Ni LDH, respectively. This increased surface area can be a key to enhanced performance for this sample. In this work, the antimicrobial properties have also been observed to differ between the samples, as will be discussed. The difference in
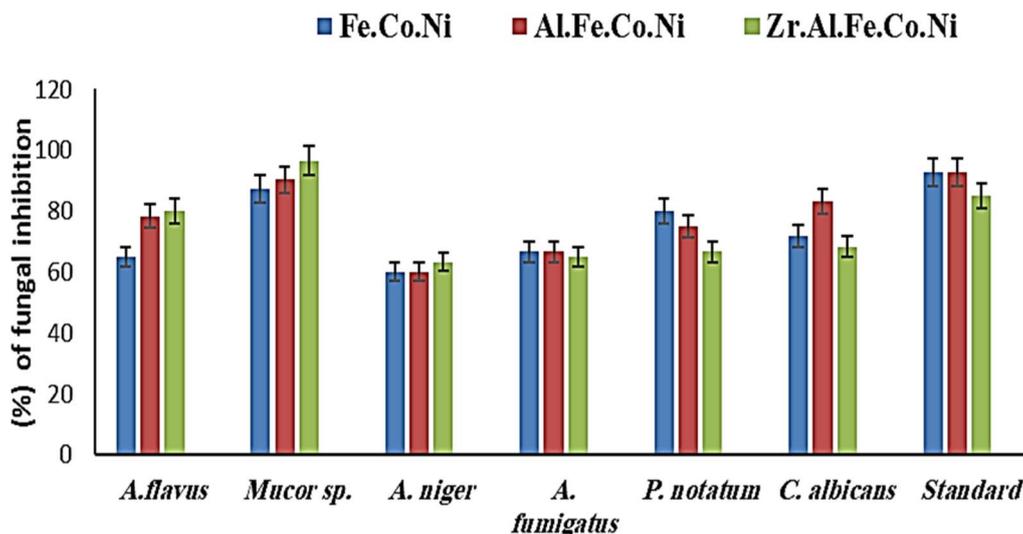
Fig. 13 Percentage of fungal inhibition by the different LDHs, Zr Al Fe Co Ni showed the best obtained inhibition percentage compared to other compounds especially against *M. indicus* in comparison to other fungal isolates.

Table 2 Semi-quantitative inhibition% of the biofilm formation for non-treated and treated bacterial and fungi pathogens with Zr Al Fe Co Ni, Al Fe Co Ni, and Fe Co Ni LDHS[a]

	OD of crystal violet stain at 570.0 nm				Inhibition%		
Test organism	Control	Treated with Fe Co Ni LDH	Treated with Al Fe Co Ni LDH	Treated with Zr Al Fe Co Ni LDH	Fe Co Ni LDH	Al Fe Co Ni LDH	Zr Al Fe Co Ni LDH
S. aureus	$0.925^{d,e} \pm 0.0070$	$0.108^e \pm 0.0051$	$0.098^c \pm 0.0053$	$0.045^f \pm 0.0055$	88.32	89.40	95.13
St. pneumoniae	$0.785^c \pm 0.0065$	$0.127^d \pm 0.0053$	$0.115^d \pm 0.0055$	$0.057^c \pm 0.0040$	83.82	85.35	92.73
L. monocytogenes	$0.656^f \pm 0.0046$	$0.125^e \pm 0.0046$	$0.134^e \pm 0.0061$	$0.079^e \pm 0.0046$	80.94	79.57	87.95
H. influenza	$0.938^a \pm 0.0065$	$0.225^{a,b} \pm 0.0045$	$0.200^{a,b} \pm 0.0051$	$0.095^b \pm 0.0047$	76.01	78.67	85.24
B. subtilis	$0.545^f \pm 0.0018$	$0.110^e \pm 0.0065$	$0.185^e \pm 0.0055$	$0.059^{e,f} \pm 0.0036$	79.81	66.05	89.17
E. coli	$0.810^b \pm 0.0080$	$0.245^{c,d} \pm 0.0041$	$0.222^{c,d} \pm 0.0053$	$0.115^f \pm 0.0055$	69.75	72.59	85.80
A. flavus	$0.777^a \pm 0.0025$	$0.315^c \pm 0.0035$	$0.375^b \pm 0.0045$	$0.215^c \pm 0.0056$	59.45	51.99	72.32
Mucor sp.	$0.770^c \pm 0.0065$	$0.355^b \pm 0.0045$	$0.375^e \pm 0.0035$	$0.205^f \pm 0.0025$	53.89	51.29	73.37
A. niger	$0.790^c \pm 0.0015$	$0.452^e \pm 0.0045$	$0.415^c \pm 0.0035$	$0.269^b \pm 0.0025$	42.78	47.46	65.94
A. fumigatus	$0.675^b \pm 0.0045$	$0.425^e \pm 0.0056$	$0.445^e \pm 0.0053$	$0.330^f \pm 0.0045$	37.03	34.07	51.11
P. notatum	$0.725^e \pm 0.0046$	$0.475^d \pm 0.0036$	$0.410^d \pm 0.0056$	$0.230^d \pm 0.0055$	34.48	43.44	68.27
C. albicans	$0.755^{d,e} \pm 0.0046$	$0.300^b \pm 0.0046$	$0.290^b \pm 0.0056$	$0.275^a \pm 0.0036$	60.26	61.58	63.57

[a] Values are means $\pm$ SD ($n = 3$). Data within the groups are analyzed using one-way analysis of variance (ANOVA) followed by [a, b, c, d, e, f] Duncan's multiple range test (DMRT).

BET surface area and any other possible characteristics of the LDH samples can originate from the effects of atomic radii, elector-negativity, and other physic–chemical properties of the constituting elements of the LDH sample.[11] Moreover, during the synthesis of LDH several factors can affect the morphology of the product including electrostatic or dipolar fields associated with hydrogen-bonds, hydrophobic interactions, crystal-face attraction, and van der Waals forces, which affects the attraction and self-assembly of the formed crystals into possible 3D geometries.[37] In this work, it was noticed that the quaternary sample has a flower-like morphology rather than a simple 2D morphology, as observed in Fig. 2b. This 3D flowery shape formed from 2D layers is assumed to be responsible for the elevated surface area of this sample, which can affect its performance in different applications. In addition, this shape has a narrow pore size distribution, as shown in Fig. 5b, which can further alter its performance compared to the other samples. This flowery shape can be attributed to the self-
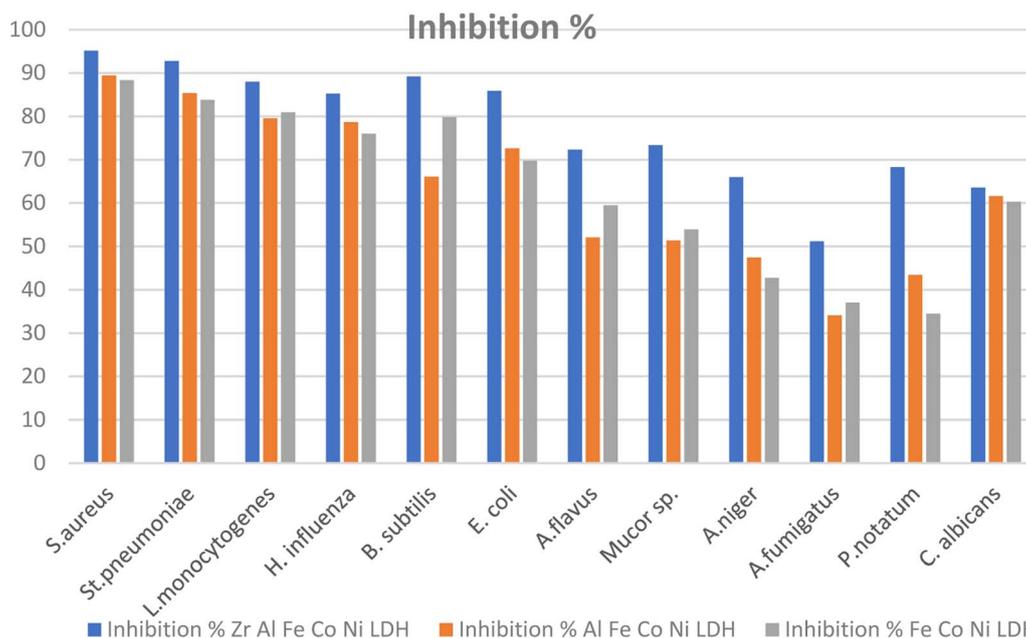
Fig. 14 Anti-biofilm potential of Zr Al Fe Co Ni, Al Fe Co Ni, and Fe Co Ni LDHs against various pathogenic microbes as inhibition%.
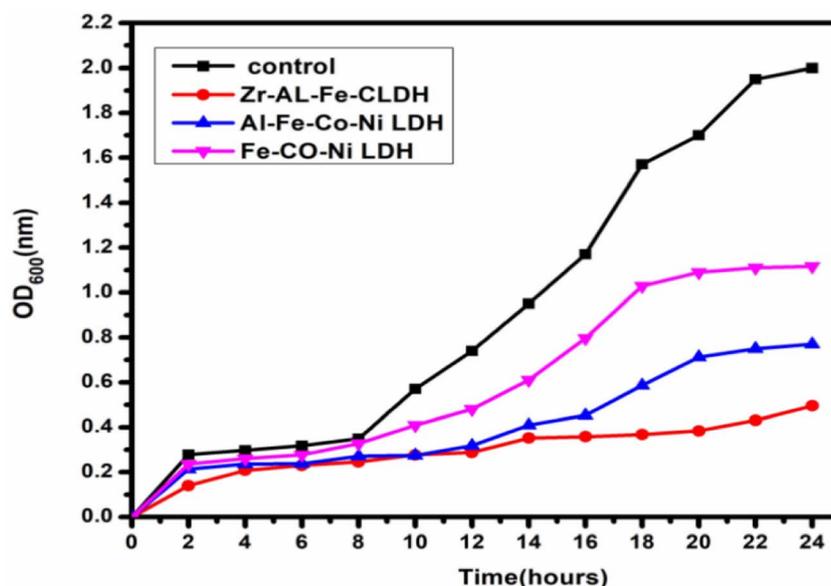

Fig. 15 The effect of Zr Al Fe Co Ni, Al Fe Co Ni, and Fe Co Ni LDHs on the growth of *S. aureus*.

assembly of the nucleated layers upon precipitation due to the presence of the aluminum cation as compared to the ternary sample lacking such a cation. When zirconium cation was further introduced, this flower-like morphology was also lost, but the layers were formed closer together compared to the ternary sample, as evident from the narrower pore size distribution shown in Fig. 5b. This shows that the chemistry of the elements involved in the preparation of LDH samples can have significant effects not only on the application level but also on the nucleation and growth steps occurring during the synthesis

procedure Fig. 2(a–c). It was found that the catalytic performance is as a result of the synergistic role of the total site densities. Small pore openings of the catalyst structure, that prevented the interaction of bacteria or fungi from reaching the catalyst's active sites.[38]

In this work, we further explore the antimicrobial properties of the prepared samples against bacterial and fungal species. To evaluate the potential biological activities of the newly synthesized LDHs, the antimicrobial properties of Fe Co Ni, Al Fe Co Ni, and Zr Al Fe Co Ni were evaluated using the determination of
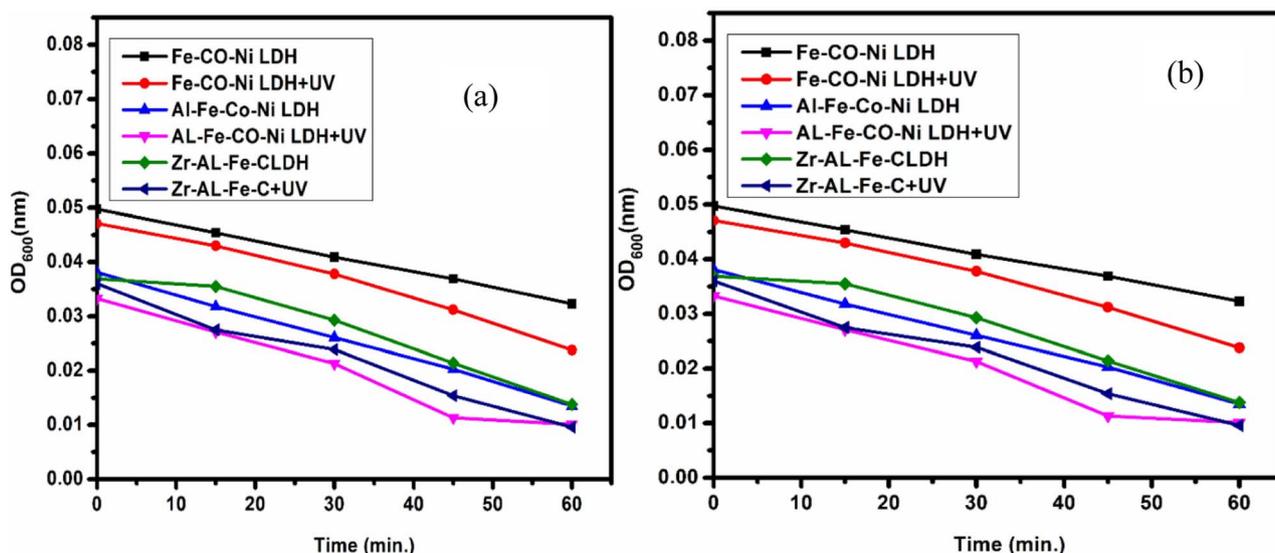
Fig. 16 (a) The effect of UV on the antibacterial activity of Zr Al Fe Co Ni, Al Fe Co Ni, and Fe Co Ni against *S. aureus*, and (b) zooming area.
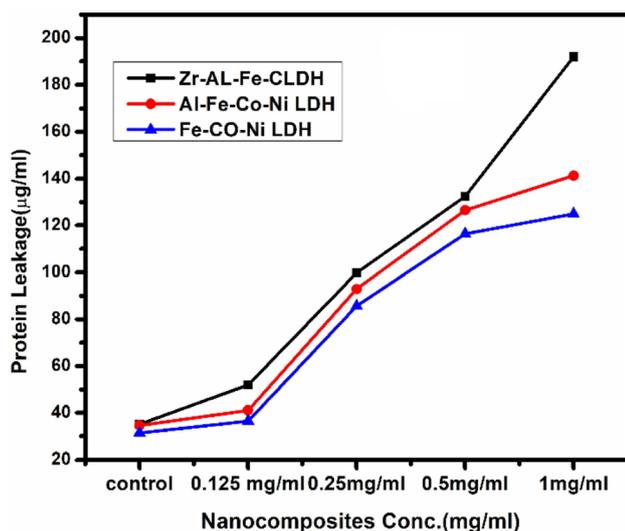

Fig. 17 The effect of Zr Al Fe Co Ni (black arrows), Al Fe Co Ni (red arrows), and Fe Co Ni (blue arrows) on the protein leakage of *S. aureus* cell membranes.

MIC, MBC, and MFC using the agar disk diffusion method. The tested bacterial and fungal species are commonly known microbial pathogens that have potential consequences for human health. To tackle these infectious organisms, it is critical to understand the MICs and MBCs of antimicrobials, whether bacteriostatic or bactericidal, in order to determine effective doses.[39] Being bio-compatible materials that are non-toxic to living tissues, LDHs have biomedical uses, including eradicating pathogenic microbes.[1] In this study, Fe Co Ni, Al Fe Co Ni, and Zr Al Fe Co Ni had different levels of *in vitro* antibacterial activity against all of the investigated microbes, and in some cases, they were stronger than the reference antibiotics. Among the three LDHs, Zr Al Fe Co Ni displayed substantial antibacterial activities against the bacterial species tested, as evidenced by the lowest MIC and MBC reported in the current study. Furthermore, significant variations were identified among strains. This could be attributed to an array of factors including infusibility, solubility, and diameters of LDHs,[40,41] the chemical structure of the cell walls of bacterial strains, and their intrinsic capabilities to resist the deleterious effects of the LDHs.[41] From biofilm results, the differences in inhibition percentage against various microbes are attributed to factors such as the greater surface area of the LDH allowing more antimicrobial component attachment, particle size effects, mode of attack, and chemical properties influencing the interaction of Zr Al Fe Co Ni with biofilm-forming microorganisms.[42]

Although the precise mechanism by which LDH demonstrated antimicrobial activity is still unknown, numerous possibilities have been proposed based on various clues. Firstly, the generation of highly reactive free radicals, hydroxyl ions, in an aqueous environment may be responsible for antimicrobial activity.[43,44] Hydroxyl radicals could react strongly with many vital bio-molecules, including proteins, lipids, and nucleic acids, generating undesired redox reactions. These events have a negative impact on the essential biological functions like membrane integrity, protein synthesis and catalysis, DNA replication, and normal cell division.[45,46] Secondly, the positive charge of LDH was increased, resulting in enhanced antibacterial action. This might be attributable to the cell wall of Gram-positive bacteria, which was formed entirely of peptide peptidoglycan, with numerous pores that allowed external molecules to enter the cell without difficulty and accelerated the absorption of ions.[47,48]

Thirdly, metal ions are presumably transported into microbial cells *via* various selective or non-selective ion-transport systems. Intracellular accumulation of the metal ions could exert potential toxic effects on microbial cells. They could interfere with bacterial membranes impairing, their integrity
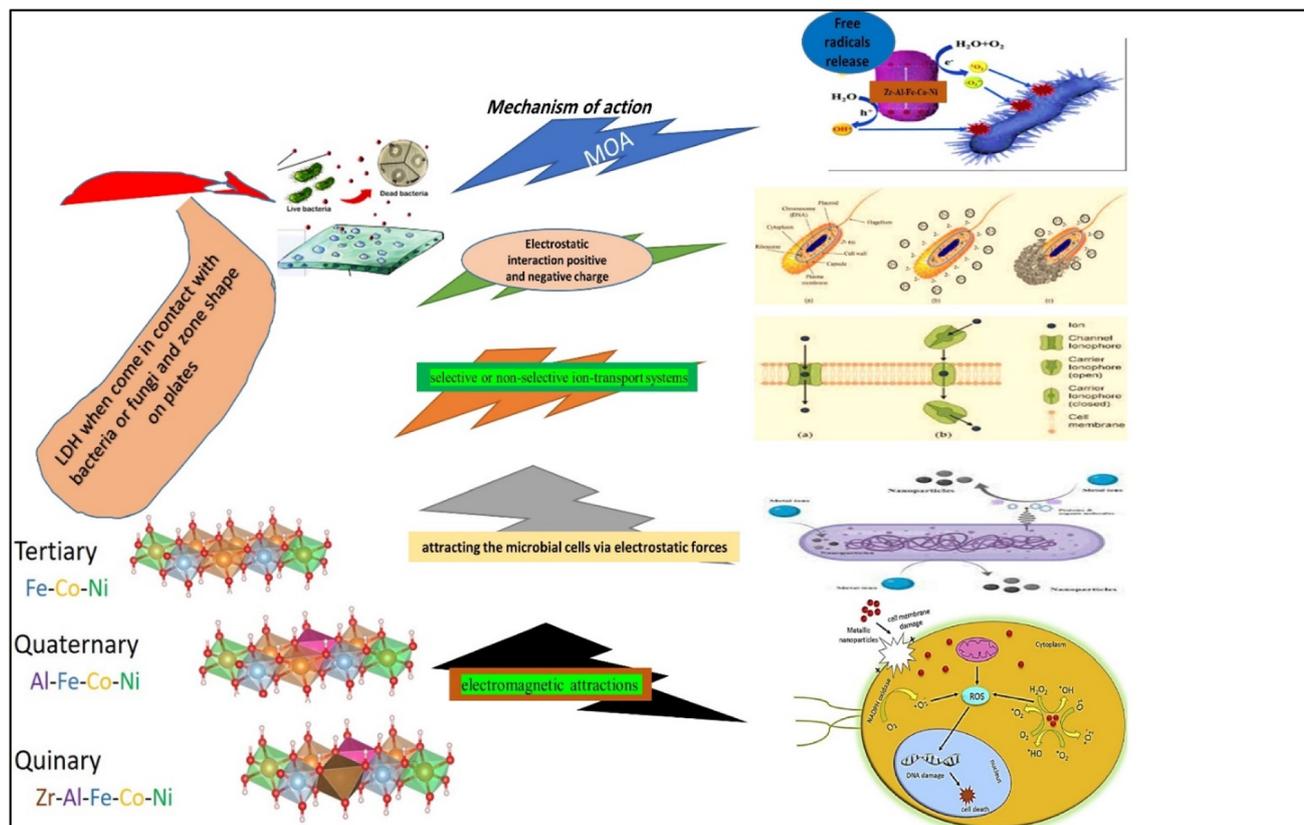
Fig. 18   A schematic diagram illustrating the possible mechanisms of action of the different LDHs on bacterial and fungal strains and isolates.

and binding with SH-group-containing vital cellular components causing their dysfunction.[44] Fourthly, LDH could exert its antimicrobial activity by attracting the microbial cells *via* electrostatic forces that prevent the adhesion and adsorption of microbial cells. Fifthly, reactive oxygen species (ROS) and free radicals produced by LDHs harm the bacterial cell wall and prevent the activity of the respiratory enzymes.[39,49] Finally, LDHs can inhibit bacterial adhesion and colonization on the surface, due to the enhanced surface hydro-phobicity and smaller surface roughness, hindering microbial biofilm formation and substantiating the susceptibility.[49,50] Nonetheless, it can be speculated that the antimicrobial properties seem to be the result of the combined actions of one or more of the above-mentioned factors. These areas establish solid bases for future research directions that need to be deciphered. It has been reported that Zr ions can inhibit bacterial adhesion and colonization on the surface due to their enhanced surface hydro-phobicity and smaller surface roughness.[51,52] In conclusion, the potential antimicrobial activity of LDHs, particularly Zr Al Fe Co Ni, against pathogenic bacteria and fungi makes them promising candidates to be further developed to minimize risks to global public health.

Furthermore, the findings of this study demonstrated that the incorporation of zirconium ions into the Zr Al Fe Co Ni LDH material leads to a notable enhancement in antimicrobial efficacy when compared to other LDH materials that were examined. It has been observed that the introduction of zirconium

ions significantly augments the antimicrobial activity. The underlying mechanism of action of zirconium has been extensively investigated in a previous study, wherein it was elucidated that the positively charged zirconium ions disrupt the negatively charged bacterial cell wall, ultimately leading to the demise of the bacterial cells. This phenomenon has been observed across various bacterial strains, highlighting the broad-spectrum antibacterial potential of zirconium. A comparable outcome was seen in the case of silver nanoparticles.[53] According to scientific communities, it has been observed that metal oxides are capable of transferring positive charges, while microorganisms possess a negative charge. This leads to electromagnetic attractions between metal oxide nanoparticles and microbes, ultimately resulting in the oxidation process and subsequent death of the microorganisms.[54] El Zowalaty *et al.*[55] conducted a synthesis of sulfated zirconia nanoparticles, which exhibited significant antibacterial efficacy against a diverse array of antibiotic-resistant bacterial strains. In a previous study, Banerjee *et al.*[56] documented the antibacterial properties of ZrO_2 nanoparticles against *E. coli* bacteria. Based on the obtained data, Fig. 18, it can be asserted that zirconium exhibits promising potential as an antibacterial agent.[57]

5   Conclusions

Zr Al Fe Co Ni LDH was shown to have superb antibacterial action, as evidenced by the lowest MIC values (4–166.7 μg

mL^{-1}). Conversely, Fe Co Ni (416 μg mL^{-1}) had a high MIC value against *A. flavus*. Therefore, this LDH has significant potential as a novel antibacterial agent, particularly in light of the persistent issue of antibiotic resistance in bacteria and fungi. Additionally, Zr Al Fe Co Ni had the greatest biofilm inhibition percentage (95.13%) against *S. aureus*, *St. pneumoniae* (93.93%) and *Mucor* sp. (73.37%) following closely after. Also, Zr Al Fe Co Ni had a significant impact on the growth curve, lowering the OD600 to 0.49. In comparison to the untreated control, Al Fe Co Ni, and Fe Co Ni LDHs, the UV assay findings demonstrated a considerable increase in bacterial and fungal growth following UV illumination of Zr Al Fe Co Ni LDH.

6 Future prospective

More advanced molecular, genetic, and different pathways are needed for a better explanation of the main mechanism of action of the studies. LDHs as antimicrobial agents, such as UV illumination on the antimicrobial and antifungal properties, anti-biofilm of the synthesized materials, kinetics study regarding the growth curve assay of the most sensitive microbes, and antimicrobial reaction mechanisms must be performed, such as membrane leakage assay, SEM imaging, high resolution transmission electron microscopy (HRTEM) imaging, and lipid peroxidation. It can be concluded that further work is required to fully understand the antibacterial and antifungal mechanisms of such complex multi-metallic LDH samples. Moreover, the synthesis, nucleation, growth mechanisms, and resultant morphology of the LDH samples need to be studied in depth as they can affect their antimicrobial properties and the antibacterial and antifungal mechanisms. Studying such multi-metallic LDH systems can pave the road towards the synthesis and application of more promising, highly efficient, and cost-effective multi-metallic 3D LDH-based nanomaterials and nanocomposites, especially in biomedical fields of research.

Abbreviations

LDH	Layered double hydroxides
Zr	Zirconium
Al	Aluminum
Fe	Iron
Co	Cobalt
Ni	Nickel
B.	*Bacillus*
E.	*Escherichia*
H.	*Haemophilus*
S.	*Staphylococcus*
St.	*Streptococcus*
AR	Antimicrobial resistance
XRD	X-ray diffractometer
FTIR	Fourier transform infrared
BET	Brunauer–Emmett–Teller
SEM	Scanning electron microscope
A.	*Aspergillus*
C.	*Candida*
MH	Muller Hinton
SD	Sabarouds dextrose
LB	Luria-Bertani
MIC	Minimum inhibitory concentration
MBC	Minimum bactericidal concentration
MFC	Minimum fungicidal concentration
CFU	Colony forming units
CV	Crystal violet
UV-Vis	Ultraviolet-visible
OD	Optical density
NB	Nutrient broth
rpm	Round per minute
ROS	Reactive oxygen species

Ethical approval

Not applicable as the study not applied on human or animals study. The article does not include any studies on human participants or animals conducted by any of the authors.

Data availability

The datasets used and/or analyzed during the current study available from the corresponding author on reasonable request.

Conflicts of interest

None of the authors have a conflict of interest to disclose.

References

1 H. Zhi, *et al.*, Layered Double Hydroxide Nanosheets Improve the Adhesion of Fungicides to Leaves and the Antifungal Performance, *ACS Appl. Nano Mater.*, 2022, **5**, 5316–5325.

2 M. Pavlovic, A. Szerlauth, S. Muráth, G. Varga and I. Szilagyi, Surface modification of two-dimensional layered double hydroxide nanoparticles with biopolymers for biomedical applications, *Adv. Drug Delivery Rev.*, 2022, **191**, 114590.

3 T. Hu, *et al.*, Layered double hydroxide-based nanomaterials for biomedical applications, *Chem. Soc. Rev.*, 2022, **51**, 6126–6176.

4 M. U. Qamar, et al., Antibiotic-Resistant Bacteria, Antimicrobial Resistance Genes, and Antibiotic Residue in Food from Animal Sources: One Health Food Safety Concern, Microorganisms, 2023, 11, 161.

5 X. Wang and T. Li, Current problems with the antibiotic-resistant bacteria and multiresistance bacteria, in Degradation of Antibiotics and Antibiotic-Resistant Bacteria from Various Sources, Elsevier, 2023, pp. 89–115.

6 R. Mahmoud, et al., Novel anti-inflammatory and wound healing controlled released LDH-Curcumin nanocomposite via intramuscular implantation, in vivo study, Arabian J. Chem., 2022, 15, 103646.

7 G. Mishra, B. Dash and S. Pandey, Layered double hydroxides: A brief review from fundamentals to application as evolving biomaterials, Appl. Clay Sci., 2018, 153, 172–186.

8 J. Awassa, D. Cornu, C. Ruby and S. El-Kirat-Chatel, Direct contact, dissolution and generation of reactive oxygen species: How to optimize the antibacterial effects of layered double hydroxides, Colloids Surf., B, 2022, 217, 112623.

9 C. Ning, et al., Review of photo- and electro-catalytic multi-metallic layered double hydroxides, Coord. Chem. Rev., 2023, 480, 215008.

10 H. Sayed, R. Mahmoud, H. F. Mohamed, Y. Gaber and N. Shehata, Co and Ni double substituted Zn-Fe layered double hydroxide as 2d nano-adsorbent for wastewater treatment, Key Eng. Mater., 2022, 922, 193–213.

11 X. Yu, et al., 2D High-Entropy Hydrotalcites, Small, 2021, 17, 2103412.

12 A. J. Knorpp, et al., Hydrothermal synthesis of multi-cationic high-entropy layered double hydroxides, RSC Adv., 2022, 12, 26362–26371.

13 S. Gao, et al., Synthesis of high-entropy alloy nanoparticles on supports by the fast moving bed pyrolysis, Nat. Commun., 2020, 11, 2016.

14 M. Kim, et al., A solution-based route to compositionally complex metal oxide structures using high-entropy layered double hydroxides, Cell Rep. Phys. Sci., 2022, 3, 100702.

15 A. A. Ahmed Anwar, R. Mahmoud, G. A. El-Fatah, A. A. Farghali and M. E. M. Hassouna, Electrochemical determination of diclofenac sodium using modified carbon paste electrode-based Zn/Fe-PANI and its efficient removal using three different layered double hydroxides, Int. J. Environ. Anal. Chem., 2023, 1–20.

16 H. Wasly, X-ray analysis for determination the crystallite size and lattice strain in zno nanoparticles, J. Al-Azhar Univ. Eng. Sect., 2018, 13, 1312–1320.

17 F. Hadacek and H. Greger, Testing of antifungal natural products: methodologies, comparability of results and assay choice, Phytochem. Anal., 2000, 11, 137–147.

18 CLSI, Reference Method for Broth Dilution Antifungal susceptibility Testing of filamentous fungi; Approved Standard—Second Edition, CLSI document M38-A2, Clinical and Laboratory Standards Institute, Wayne, PA, 2008.

19 Y. A. Jeff-Agboola, In vitro antifungal activities of essential oil from Nigerian medicinal plants against toxigenic Aspergillus flavus, J. Med. Plants Res., 2012, 6(23), 4048–4056.

20 G. D. Christensen, W. A. Simpson, A. L. Bisno and E. H. Beachey, Adherence of slime-producing strains of Staphylococcus epidermidis to smooth surfaces, Infect. Immun., 1982, 37, 318–326.

21 M. A. Ansari, H. M. Khan, A. A. Khan, S. S. Cameotra and R. Pal, Antibiofilm efficacy of silver nanoparticles against biofilm of extended spectrum β-lactamase isolates of E. coli and Klebsiella pneumoniae, Appl. Nanosci., 2014, 4, 859–868.

22 A. I. El-Batal, G. S. El-Sayyad, N. E. Al-Hazmi and M. Gobara, Antibiofilm and Antimicrobial Activities of Silver Boron Nanoparticles Synthesized by PVP Polymer and Gamma Rays Against Urinary Tract Pathogens, J. Cluster Sci., 2019, 30, 947–964.

23 M. A. Ansari, H. M. Khan, A. A. Khan, S. S. Cameotra and R. Pal, Antibiofilm efficacy of silver nanoparticles against biofilm of extended spectrum β-lactamase isolates of E. coli and Klebsiella pneumoniae, Appl. Nanosci., 2014, 4, 859–868.

24 W. Huang, J.-Q. Wang, H.-Y. Song, Q. Zhang and G.-F. Liu, Chemical analysis and in vitro antimicrobial effects and mechanism of action of Trachyspermum copticum essential oil against E. coli, Asian Pac. J. Trop. Med., 2017, 10, 663–669.

25 M. Bekhit, S. H. El-Sabbagh, R. M. Mohamed, G. S. El-Sayyad and R. Sokary, Mechanical, thermal and antimicrobial properties of LLDPE/EVA/MMT/Ag nanocomposites films synthesized by gamma irradiation, J. Inorg. Organomet. Polym. Mater., 2021, 1–15.

26 M. Abd Elkodous, et al., Enhanced photocatalytic and antimicrobial performance of a multifunctional Cu-loaded nanocomposite under UV light: theoretical and experimental study, Nanoscale, 2022, 14, 8306–8317.

27 A. N. El-Shazly, et al., Superior visible light antimicrobial performance of facet engineered cobalt doped TiO2 mesocrystals in pathogenic bacterium and fungi, Sci. Rep., 2021, 11, 5609.

28 H. Agarwal, A. Nakara, S. Menon and V. Shanmugam, Eco-friendly synthesis of zinc oxide nanoparticles using Cinnamomum Tamala leaf extract and its promising effect towards the antibacterial activity, J. Drug Delivery Sci. Technol., 2019, 53, 101212.

29 R. A. Sayed, S. E. Abd El Hafiz, N. Gamal, Y. GadelHak and W. M. A. El Rouby, Co-Fe layered double hydroxide decorated titanate nanowires for overall photoelectrochemical water splitting, J. Alloys Compd., 2017, 728, 1171–1179.

30 M. Huang, et al., Self-Assembly of Mesoporous Nanotubes Assembled from Interwoven Ultrathin Birnessite-type MnO2 Nanosheets for Asymmetric Supercapacitors, Sci. Rep., 2014, 4, 3878.

31 R. Mahmoud, H. F. M. Mohamed, S. H. M. Hafez, Y. M. Gadelhak and E. E. Abdel-Hady, Valorization of spent double substituted Co–Ni–Zn–Fe LDH wastewater nanoadsorbent as methanol electro-oxidation catalyst, Sci. Rep., 2022, 12, 19354.

32 R. M. Amin, et al., Gamma radiation as a green method to enhance the dielectric behaviour, magnetization,

antibacterial activity and dye removal capacity of Co–Fe LDH nanosheets, *RSC Adv.*, 2019, **9**, 32544–32561.

33 G. Y. Abo El-Reesh, A. A. Farghali, M. Taha and R. K. Mahmoud, Novel synthesis of Ni/Fe layered double hydroxides using urea and glycerol and their enhanced adsorption behavior for Cr (VI) removal, *Sci. Rep.*, 2020, **10**, 587.

34 M. Thommes, *et al.*, Physisorption of gases, with special reference to the evaluation of surface area and pore size distribution (IUPAC Technical Report), *Pure Appl. Chem.*, 2015, **87**, 1051–1069.

35 A. I. El-Batal, G. S. El-Sayyad, N. E. Al-Hazmi and M. Gobara, Antibiofilm and Antimicrobial Activities of Silver Boron Nanoparticles Synthesized by PVP Polymer and Gamma Rays Against Urinary Tract Pathogens, *J. Cluster Sci.*, 2019, **30**, 947–964.

36 A. I. El-Batal, H. G. Nada, R. R. El-Behery, M. Gobara and G. S. El-Sayyad, Nystatin-mediated bismuth oxide nano-drug synthesis using gamma rays for increasing the antimicrobial and antibiofilm activities against some pathogenic bacteria and *Candida* species, *RSC Adv.*, 2020, **10**, 9274–9289.

37 E. Boccalon, G. Gorrasi and M. Nocchetti, Layered double hydroxides are still out in the bloom: Syntheses, applications and advantages of three-dimensional flower-like structures, *Adv. Colloid Interface Sci.*, 2020, **285**, 102284.

38 J. Abd Rahman, A. Ramli, K. Jumbri and Y. Uemura, Tailoring the surface area and the acid–base properties of Zro2 for biodiesel production from Nannochloropsis sp., *Sci. Rep.*, 2019, **9**, 16223.

39 N. T. T. Vy, *et al.*, Drug-Intercalated Zn–Al-Layered Double Hydroxides as Antibacterial and Anti-inflammatory Delivery Systems for Wound Healing Applications, *J. Cluster Sci.*, 2023, **34**, 2619–2632.

40 J. Awassa, *et al.*, Divalent metal release and antimicrobial effects of layered double hydroxides, *Appl. Clay Sci.*, 2022, **216**, 106369.

41 A. L. M. D. De Sousa, *et al.*, Layered Double Hydroxides as Promising Excipients for Drug Delivery Purposes, *Eur. J. Pharm. Sci.*, 2021, **165**, 105922.

42 P. P. Mahamuni, *et al.*, Synthesis and characterization of zinc oxide nanoparticles by using polyol chemistry for their antimicrobial and antibiofilm activity, *Biochem. Biophys. Rep.*, 2019, **17**, 71–80.

43 T. Sadeghi Rad, *et al.*, Graphene-based ZnCr layered double hydroxide nanocomposites as bactericidal agents with high sonophotocatalytic performances for degradation of rifampicin, *Chemosphere*, 2022, **286**, 131740.

44 A. A. G. El-Shahawy, F. I. Abo El-Ela, N. A. Mohamed, Z. E. Eldine and W. M. A. El Rouby, Synthesis and evaluation of layered double hydroxide/doxycycline and cobalt ferrite/chitosan nanohybrid efficacy on gram positive and gram negative bacteria, *Mater. Sci. Eng., C*, 2018, **91**, 361–371.

45 C. Madhusha, *et al.*, A Novel Green Approach to Synthesize Curcuminoid-Layered Double Hydroxide Nanohybrids: Adroit Biomaterials for Future Antimicrobial Applications, *ACS Omega*, 2021, **6**, 9600–9608.

46 G. Francius, E. André, S. Soulé, C. Merlin and C. Carteret, Layered Double Hydroxides (LDH) as nanocarriers for antimicrobial chemotherapy: From formulation to targeted applications, *Mater. Chem. Phys.*, 2023, **293**, 126965.

47 G. Mosconi, *et al.*, Antimicrobial modification of polypropylene films by photograft and layered double hydroxides assembly, *React. Funct. Polym.*, 2022, **178**, 105349.

48 S. Malekkhaiat Häffner, *et al.*, Membrane interactions and antimicrobial effects of layered double hydroxide nanoparticles, *Phys. Chem. Chem. Phys.*, 2017, **19**, 23832–23842.

49 A. Donnadio, *et al.*, Bioinspired Reactive Interfaces Based on Layered Double Hydroxides-Zn Rich Hydroxyapatite with Antibacterial Activity, *ACS Biomater. Sci. Eng.*, 2021, **7**, 1361–1373.

50 E. N. Alkhafaji, N. A. Oda and L. M. Ahmad, Characterization of silver nanohybrid with layers double hydroxide and demonstration inhibition of antibiotic-resistance S. aureus, *Egypt. J. Chem.*, 2022, **65**(6), 143–157.

51 G. Yi, *et al.*, Surface Antimicrobial Treatment by Biocompatible, Vertically Aligned Layered Double Hydroxide Array, *Adv. Mater. Interfaces*, 2022, **9**, 2101872.

52 C. Balcik, *et al.*, Development of ZnFeCe Layered Double Hydroxide Incorporated Thin Film Nanocomposite Membrane with Enhanced Separation Performance and Antibacterial Properties, *Water*, 2023, **15**, 264.

53 R. Emmanuel, *et al.*, Antimicrobial efficacy of green synthesized drug blended silver nanoparticles against dental caries and periodontal disease causing microorganisms, *Mater. Sci. Eng., C*, 2015, **56**, 374–379.

54 H. Zhang and G. Chen, Potent antibacterial activities of Ag/TiO2 nanocomposite powders synthesized by a one-pot sol−gel method, *Environ. Sci. Technol.*, 2009, **43**, 2905–2910.

55 A. Mftah, *et al.*, Physicochemical properties, cytotoxicity, and antimicrobial activity of sulphated zirconia nanoparticles, *Int. J. Nanomed.*, 2015, 765–774.

56 K. Banerjee, M. Prithviraj, N. Augustine, S. P. Pradeep and P. Thiagarajan, Analytical characterization and antimicrobial activity of nano zirconia particles, *J. Chem. Pharm. Sci.*, 2016, **9**, 1186–1190.

57 S. Sreevidya, *et al.*, Phyto-nano-MgO quantum dots by ultrasonic formulation for evaluation of toxin In-Vivo/Vitro/Silico sequels, *Chem. Eng. J.*, 2024, **483**, 149089.